

SERI/TR-215-3087
DE87012273

August 1987

A Quasi-Physical Model for Converting Hourly Global Horizontal to Direct Normal Insolation

Eugene L. Maxwell



SERI

Solar Energy Research Institute

A Division of Midwest Research Institute

1617 Cole Boulevard
Golden, Colorado 80401-3393

Operated for the

U.S. Department of Energy

under Contract No. DE-AC02-83CH10093

SERI/TR-215-3087
UC Category: 62, 63
DE87012273

A Quasi-Physical Model for Converting Hourly Global Horizontal to Direct Normal Insolation

Eugene L. Maxwell

August 1987

Prepared under Task No. 6003.100

Solar Energy Research Institute

A Division of Midwest Research Institute

1617 Cole Boulevard
Golden, Colorado 80401-3393

Prepared for the

U.S. Department of Energy

Contract No. DE-AC02-83CH10093

NOTICE

This report was prepared as an account of work sponsored by the United States Government. Neither the United States nor the United States Department of Energy, nor any of their employees, nor any of their contractors, subcontractors, or their employees, makes any warranty, expressed or implied, or assumes any legal liability or responsibility for the accuracy, completeness or usefulness of any information, apparatus, product or process disclosed, or represents that its use would not infringe privately owned rights.

Printed in the United States of America
Available from:
National Technical Information Service
U.S. Department of Commerce
5285 Port Royal Road
Springfield, VA 22161

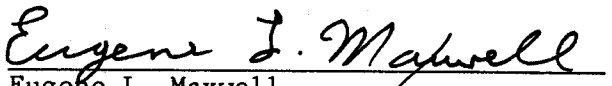
Price: Microfiche A01
Printed Copy A04

Codes are used for pricing all publications. The code is determined by the number of pages in the publication. Information pertaining to the pricing codes can be found in the current issue of the following publications, which are generally available in most libraries: *Energy Research Abstracts (ERA)*; *Government Reports Announcements and Index (GRA and I)*; *Scientific and Technical Abstract Reports (STAR)*; and publication NTIS-PR-360 available from NTIS at the above address.

PREFACE

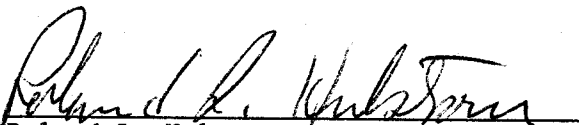
This report provides an overview of previous models developed to convert global horizontal irradiance data to direct normal irradiance data. Research performed under this task on the development of an improved model is described along with a brief discussion of work performed by others. The resultant Direct Insolation Simulation Code (DISC) is described along with the results of verification and validation tests, which are compared with the performance of the Ersatz Typical Meteorological Year (ETMY) model when applied to the exact same data sets.

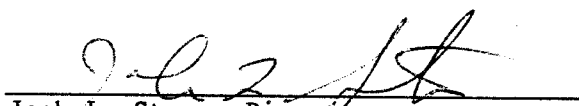
The author is grateful for the support and encouragement given by Roland Hulstrom, who provides SERI's leadership for the Resource Assessment Program. Special recognition is given to Dr. C.G. Justus of the Georgia Institute of Technology who provided the research data set for Atlanta, vital to the development of this model. The research conducted by Professor John Garrison, San Diego State University, is also recognized since it provided some direction toward the initial research effort. I also want to give special recognition to Dick Bird whose simple clear sky model generates input for the DISC model, and who provided assistance toward its development. Recognition is also given to Martin Rymes and Archie Mott for preparation of data sets, to Lakes Ismailidis for laborious data processing, to Paula Natale for typing the numerous drafts of this report and to the technical reviewers (Drs. Jeter, Garrison, Randall, and Iqbal) whose comments led to significant improvements in this report.


Eugene L. Maxwell
Senior Scientist

Approved for

SOLAR ENERGY RESEARCH INSTITUTE


Roland L. Hulstrom, Manager
Resource Assessment and Instrumentation
Branch


Jack L. Stone, Director
Solar Electric Research Division

SUMMARY

Objective

To develop an improved, physically based model for converting global horizontal insolation data to direct normal insolation data. This model will be used to upgrade direct normal data in the national historical data bases.

Discussion

During the mid-1970s, the Aerospace Direct Insolation Prediction Algorithm (ADIPA) and the Ersatz Typical Meteorological Year (ETMY) simplified version of ADIPA were used to generate all of the direct normal insolation data in the national solar radiation and meteorological (SOLMET) data bases. Measured global horizontal data were the only input to the models. Evaluations of these models and the data they produced have shown serious deficiencies (e.g., errors in hourly values as great as 70% and errors in annual means of daily total insolation approaching 20%). In general, comparisons with recent measured data showed the model generated low values under clear-sky conditions and high values under partly cloudy conditions. Furthermore, the differences exhibit large diurnal variations associated with air-mass changes.

In parametric studies of the direct normal transmittance (K_n) and the effective global horizontal transmittance (K_t), air mass is the dominant parameter affecting the relationship between these two variables. The DISC model developed under this project uses an exponential function, parametric in K_t , relating changes in K_n (ΔK_n) to air mass. Clear-sky transmittance values (K_{n_c}) were calculated using a physical model. Then the effect of clouds, water vapor, and turbidity on ΔK_n were related to air mass and K_t .

Like the ADIPA and ETMY models, global horizontal insolation is the only input to the current version of the DISC model. Future versions will use cloud cover, water vapor, albedo, and turbidity (when available) to improve the accuracy of modeled estimates of direct normal insolation. We evaluated the performance of the current model using data from four locations with widely differing latitudes and climates.

Conclusions

Comparisons between measured and modeled data at Atlanta, Ga; Brownsville, Tex.; Albuquerque, N.M.; and Bismarck, N.D., show that RMS errors for the DISC model are significantly improved over the results obtained with the ETMY model. This improvement probably resulted from the effective use of air mass to track diurnal variations in insolation. The mean bias errors are similar for the two models. Of greatest significance is the improved performance of the DISC model, accomplished without compensating for seasonal, climatic, or geographic differences.

TABLE OF CONTENTS

	<u>Page</u>
1.0 Introduction.....	1
2.0 Previous Models and Related Research.....	2
2.1 ADIPA and ETMY Models.....	2
2.1.1 Model Descriptions.....	2
2.1.2 Performance of the ADIPA and ETMY Models.....	4
2.2 Related Research.....	5
3.0 Development of the Model.....	10
3.1 Direct Normal versus Global Horizontal Relationships.....	10
3.1.1 Seasonal, Annual, and Climate Relations.....	10
3.1.2 Multiple Correlation Studies.....	11
3.1.3 Parametric Studies.....	13
3.2 Developing the Algorithms.....	20
3.2.1 Establishing Clear-Sky Limits.....	21
3.2.2 Deriving the Functional Relationships Between ΔK_n and Air Mass.....	21
3.2.3 Coefficient Functions.....	30
3.3 Description of the Model.....	33
4.0 Verification and Validation of the Model.....	36
4.1 Methods of Analysis.....	36
4.2 Verification Results.....	37
4.3 Validation Results.....	41
4.3.1 Results for Brownsville, Texas.....	41
4.3.2 Results for Albuquerque, New Mexico.....	44
4.3.3 Results for Bismarck, North Dakota.....	44
5.0 Conclusions and Future Research.....	52
5.1 Verification and Validation Results.....	52
5.2 Future Research.....	53
6.0 References.....	54

LIST OF FIGURES

	<u>Page</u>
2-1 Scatter Plot of Observed Hourly Values of Kn vs. Kt for Maynard, Mass. (1976).....	3
2-2 Five Station Means and Station Extreme Values of the Segmented Relationship between Kn and Kt (all months).....	4
2-3 One-Minute Data and ETMY (Modeled Minus Observed) Differences for Hourly Means of Direct Normal Insolation for Albany, N.Y., on April 21, 1979.....	6
2-4 One-Minute Data and ETMY (Modeled Minus Observed) Differences for Hourly Means of Direct Normal Insolation for Atlanta, Ga., on June 28, 1981.....	7
2-5 Mean Kd Values vs. Kt for Summer Conditions (Data from 33 stations of the new NOAA network).....	8
2-6 Mean Kd Values vs. Kt for Winter Conditions (Data from 33 stations of the new NOAA network).....	9
3-1 Observed Seasonal Changes in the Relationship between Kn and Kt (Third-order regression fits to three years of data from Atlanta, Ga.).....	11
3-2 Observed Annual Changes in the Relationship between Kn and Kt (Third-order regression fits to data for March, April, and May from Las Vegas, Nev.).....	12
3-3 Observed Differences in the Relationship between Kn and Kt Possibly Caused by Climate Differences. [Third-order regression fits to three years of summer (July and August) data for the six locations indicated].....	12
3-4 Scatter Plots of Kn vs. Kt for Four Subsets of Data from Atlanta, Ga. (October 1981).....	18
3-5 Scatter Plots of ΔKn vs. ΔKt for Four Subsets of Data from Atlanta, Ga. (October 1981).....	18
3-6 Scatter Plot of Kn vs. Kt for Medium Air Mass (4.0 to 6.0) and Low Cloud Cover (0 to 0.2) for Data from Atlanta, Ga. (October 1981).....	19
3-7 Scatter Plot of Kn vs. Kt for Medium Air Mass (4.0 to 6.0) and Low Precipitable Water Vapor (0.0 to 1.5 cm) for Data from Atlanta, Ga. (October 1981).....	19

LIST OF FIGURES (Continued)

	<u>Page</u>
3-8 Scatter Plots of K_d and $\langle K_d \rangle$ vs. K_t for Similar Hourly and Average Seasonal Conditions, Respectively.....	20
3-9 Scatter Plot of K_d and $\langle K_d \rangle$ vs. K_t for Similar Hourly and Average Seasonal Conditions, Respectively.....	21
3-10 K_n vs. Air Mass Calculated for Clear, Dry Conditions (Turbidity = 0.03 and Precipitable Water Vapor = 0.2 cm) Using Bird's Clear-Sky Model.....	22
3-11(a) Scatter Plots of ΔK_n vs. Air Mass and Exponential Fits for an Atlanta Data Subset ($0.23 < K_t < 0.27$) Used in Developing the Algorithms for the DISC Model.....	23
3-11(b) Scatter Plots of ΔK_n vs. Air Mass and Exponential Fits for an Atlanta Data Subset ($0.28 < K_t < 0.32$) Used in Developing the Algorithms for the DISC Model.....	23
3-11(c) Scatter Plots of ΔK_n vs. Air Mass and Exponential Fits for an Atlanta Data Subset ($0.33 < K_t < 0.37$) Used in Developing the Algorithms for the DISC Model.....	24
3-11(d) Scatter Plots of ΔK_n vs. Air Mass and Exponential Fits for an Atlanta Data Subset ($0.38 < K_t < 0.42$) Used in Developing the Algorithms for the DISC Model.....	24
3-11(e) Scatter Plots of ΔK_n vs. Air Mass and Exponential Fits for an Atlanta Data Subset ($0.43 < K_t < 0.47$) Used in Developing the Algorithms for the DISC Model.....	25
3-11(f) Scatter Plots of ΔK_n vs. Air Mass and Exponential Fits for an Atlanta Data Subset ($0.48 < K_t < 0.52$) Used in Developing the Algorithms for the DISC Model.....	25
3-11(g) Scatter Plots of ΔK_n vs. Air Mass and Exponential Fits for an Atlanta Data Subset ($0.53 < K_t < 0.57$) Used in Developing the Algorithms for the DISC Model.....	26
3-11(h) Scatter Plots of ΔK_n vs. Air Mass and Exponential Fits for an Atlanta Data Subset ($0.58 < K_t < 0.62$) Used in Developing the Algorithms for the DISC Model.....	26
3-11(i) Scatter Plots of ΔK_n vs. Air Mass and Exponential Fits for an Atlanta Data Subset ($0.63 < K_t < 0.67$) Used in Developing the Algorithms for the DISC Model.....	27
3-11(j) Scatter Plots of ΔK_n vs. Air Mass and Exponential Fits for an Atlanta Data Subset ($0.68 < K_t < 0.72$) Used in Developing the Algorithms for the DISC Model.....	27

LIST OF FIGURES (Continued)

	<u>Page</u>
3-11(k) Scatter Plots of ΔK_n vs. Air Mass and Exponential Fits for an Atlanta Data Subset ($0.73 < K_t < 0.77$) Used in Developing the Algorithms for the DISC Model.....	28
3-11(1) Scatter Plots of ΔK_n vs. Air Mass and Exponential Fits for an Atlanta Data Subset ($0.77 < K_t < 0.83$) Used in Developing the Algorithms for the DISC Model.....	28
3-12 Thirteen Exponential Functions Relating ΔK_n and Air Mass.....	29
3-13 An Enlarged View of the High K_t Functions Relating ΔK_n and Air Mass.....	31
3-14 An Enlarged View of the Low K_t Functions Relating ΔK_n and Air Mass.....	31
3-15 Coefficient a (from the Exponential Functions Relating ΔK_n and Air Mass) and the Two Polynomial Functions Fit to the a Data.....	32
3-16 Coefficient b (from the Exponential Functions Relating ΔK_n and Air Mass) and the Two Polynomial Functions Fit to the b Data.....	32
3-17 Coefficient c (from the Exponential Functions Relating ΔK_n and Air Mass) and the Two Polynomial Functions Fit to the c Data.....	33
3-18 Block Diagram of the DISC Model for Estimating Direct Normal Insolation from Observed Global Horizontal Insolation Data.....	34
4-1 Percent RMS Differences between Estimated (DISC and ETMY Models) and Observed Direct Normal Insolation Values for 1981 Data from Atlanta, Ga.....	38
4-2 Percent Mean Bias Differences between Estimated (DISC and ETMY Models) and Observed Direct Normal Insolation Values for 1981 Data from Atlanta, Ga.....	38
4-3 Percentage of All Hours for Which Clear (0 to 0.1), Scattered (0.4 to 0.6), and Overcast (0.9 to 1.0) Cloud-Cover Conditions Were Observed at Atlanta in 1981.....	39
4-4 Estimated (ETMY and DISC Models) Minus Observed Differences in Hourly Means of Direct Normal Insolation from Atlanta, Ga., on June 14, 1981 (Clear-sky conditions).....	40
4-5 Estimated (ETMY and DISC Models) Minus Observed Differences in Hourly Means of Direct Normal Insolation from Atlanta, Ga., on June 28, 1981 (Scattered-cloud conditions).....	40

LIST OF FIGURES (Continued)

	<u>Page</u>	
4-6	Percent Mean Bias Differences between Estimated (DISC and ETMY Models) and Observed Direct Normal Insolation Values for 1980 Data from Brownsville, Tex.....	42
4-7	Percent RMS Differences between Estimated (DISC and ETMY Models) and Observed Direct Normal Insolation Values for 1980 Data for Brownsville, Tex.....	42
4-8	Percentage of All Hours for Which Clear (0 to 0.1), Scattered (0.4 to 0.6), and Overcast (0.9 to 1.0) Cloud-Cover Conditions Were Observed at Brownsville in 1980.....	43
4-9	Estimated (ETMY and DISC Models) Minus Observed Differences in Hourly Means of Direct Normal Insolation for Brownsville, Tex., on January 23, 1980 (0.7 to 1.0 cloud cover).....	43
4-10	Percent Mean Bias Differences between Estimated (DISC and ETMY Models) and Observed Direct Normal Insolation Values for 1979 Data for Albuquerque, N.M.....	45
4-11	Percentage of All Hours for Which Clear (0 to 0.1), Scattered (0.4 to 0.6), and Overcast (0.9 to 1.0) Cloud-Cover Conditions Were Observed at Albuquerque in 1979.....	45
4-12	Percent RMS Differences between Estimated (DISC and ETMY Models) and Observed Direct Normal Insolation Values for 1979 Data from Albuquerque, N.M.....	46
4-13	Estimated (ETMY and DISC Models) Minus Observed Differences in Hourly Means of Direct Normal Insolation for Albuquerque, N.M., on October 6, 1979 (Clear-sky conditions).....	46
4-14	Estimated (ETMY and DISC Models) Minus Observed Differences in Hourly Means of Direct Normal Insolation for Albuquerque, N.M., on October 9, 1979 (0.3 to 0.9 cloud cover).....	47
4-15	Percent Mean Bias Differences between Estimated (DISC and ETMY Models) and Observed Direct Normal Insolation Values for 1980 Data from Bismarck, N.D.....	47
4-16	Percent RMS Differences between Estimated (DISC and ETMY Models) and Observed Direct Normal Insolation Values for 1980 Data for Bismarck, N.D.....	48
4-17	Percentage of All Hours for Which Clear (0 to 0.1), Scattered (0.4 to 0.6), and Overcast (0.9 to 1.0) Cloud-Cover Conditions were Observed at Bismarck in 1980.....	48

LIST OF FIGURES (Concluded)

	<u>Page</u>
4-18 Estimated (ETMY and DISC Models) Minus Observed Differences in Hourly Means of Direct Normal Insolation from Bismarck, N.D., on February 27, 1980 (0.9 to 1.0 cloud cover, probable snow cover on the ground).....	49
4-19 Estimated (ETMY and DISC Models) Minus Observed Differences in Hourly means of Direct Normal Insolation from Bismarck, N.D., on February 26, 1980 (Clear-sky conditions, probable snow cover on the ground).....	49
4-20 Global, Diffuse, and Direct Irradiance at Bismarck, N.D., on February 27, 1980.....	50

LIST OF TABLES

	<u>Page</u>
3-1 Multiple Correlations for Atlanta Data Grouped by Solar Elevation (October 1981).....	14
3-2 Statistics for Atlanta Data (October 1981).....	16
3-3 Multiple Correlations of Atlanta Data with Less Than 10% Cloud Cover (October 1981).....	16
3-4 Variable Ranges Used To Form Data Subsets.....	17
3-5 Functions Relating ΔK_n and Air Mass (X).....	30

1.0 INTRODUCTION

Before 1976, very few measurements were taken of the irradiance coming directly from the solar disc (i.e., direct normal insolation). Direct normal insolation data covering a 12-month period were available for only five stations in the United States: Albuquerque, N.M.; Fort Hood, Tex.; Livermore, Calif.; Maynard, Mass.; and Raleigh, N.C. Under these circumstances, modeling was the only method available to develop a direct normal insolation data base for the United States. Randall and Whitson (1977) developed a procedure for estimating hourly direct normal insolation from hourly global horizontal insolation data. The National Oceanographic and Atmospheric Administration (NOAA) used these models to generate all of the direct normal data contained in the National SOLMET and Ersatz data bases (SOLMET, 1978).

Since 1976, direct normal data from an average of 25 months have been collected at some 70 locations in the United States (Maxwell 1987). Although this represents an increase of two orders of magnitude in available direct normal data, far more data are needed for siting and estimating the performance of large systems such as solar power plants. Because of the cost and the difficulties encountered when measuring direct normal irradiance, the solar industry may never obtain enough measured direct normal data to avoid using model estimates. Therefore, because of known shortcomings in the models used to build the SOLMET/Ersatz data bases (Hall et al. 1980; Randall and Bird 1987; and Maxwell and Bird 1987), we endeavored to develop an improved model for converting global horizontal data to direct normal data.

This report describes research performed to develop a new model, and it also briefly discusses the previous models used to create the national direct normal data bases and related research which marked the path for the development of an improved model. The results of the verification and validation of this model are compared with similar results for previous models.

Previous models were developed using empirical data-fitting techniques and employed limited physical relationships. One of the objectives of this work was to use physical principles in developing the model, assuming this would reduce the differences between modeled and measured values. Although a purely physical model was impossible, a physical algorithm is employed, and the model is based on physical principles. Therefore, this model is designated as being a quasi-physical model.

2.0 PREVIOUS MODELS AND RELATED RESEARCH

A number of physical models have been developed that require input data for cloud cover, turbidity, precipitable water vapor, ozone, and surface albedo. Data for all of these variables, based on hourly observations, are available for only limited periods from a few U.S. stations. Of these variables, many meteorological stations collect data only for cloud cover, and some solar radiation stations collect data for none of them. Therefore, our objective was to obtain a model that requires only global horizontal insolation data as input, and these physical models became irrelevant. The only relevant models that existed were those used to generate the direct normal data contained in the SOLMET/Ersatz data bases. These models are the Aerospace Direct Insolation Prediction Algorithm (ADIPA), developed by Randall and Whitson (1977) (see also Randall and Biddle 1981), and a simplified and modified version of this model called the ETMY, which was used to generate direct normal data for the Typical Meteorological Year (TMY) data sets of the Ersatz data base.

2.1 ADIPA and ETMY Models

2.1.1 Model Descriptions

Randall and Whitson obtained direct normal and global horizontal data from five stations: Albuquerque, N.M.; Fort Hood, Tex.; Livermore, Calif.; Maynard, Mass.; and Raleigh, N.C. With these data, the direct beam and global horizontal effective transmittance values were calculated according to the expressions

$$K_n = I_n / I_o , \quad (2-1)$$

and

$$K_t = I_t / (I_o \cos z) , \quad (2-2)$$

where

I_n = direct normal irradiance at the surface of the earth

I_t = total global horizontal irradiance

I_o = extraterrestrial direct normal irradiance

z = solar zenith angle

K_n = direct beam transmittance

and

K_t = effective global horizontal transmittance,

which is often referred to as the clearness or cloudiness index.

During the development of the ADIPA and ETMY models, scatter plots of K_n versus K_t , such as that shown in Figure 2-1, were prepared for each of the five stations and for a composite of all five. The relationship between K_n and K_t was determined by an incremental empirical approach rather than by a regression fit to a single functional form. The K_n - K_t data pairs were segmented into ten bins based on K_t values, beginning at 0.05 and increasing in increments of 0.1 up to 0.95. The mean values of K_n were calculated for

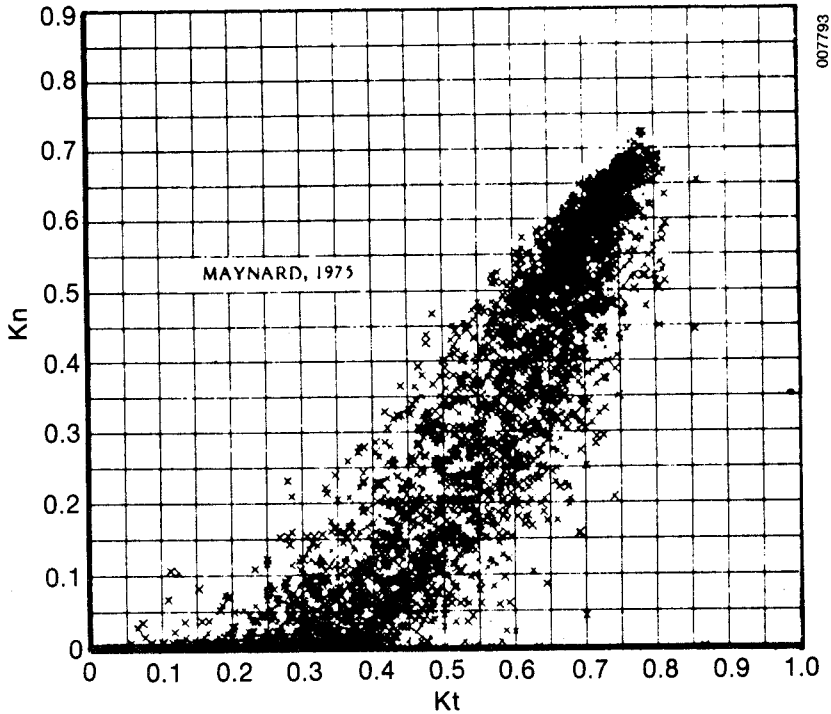


Figure 2-1. Scatter Plot of Observed Hourly Values of K_n vs. K_t for Maynard, Mass. (1976)
 Source: Randall and Whitson 1977.

each K_t bin, and these were plotted and connected with straight lines, as shown on Figure 2-2, to create a continuous relationship between K_n and K_t . Randall and Whitson found significant variations in the relationship between K_n and K_t as a function of season, but they concluded that variations between stations were not significant. Therefore, the estimation algorithm used different incremental relationships for each month but the same relationships for all stations.

The final algorithm for calculating direct normal irradiance took the form

$$I_n = I_o \tau(z) [g(K_t, m) + y(K_t, \chi)] , \tag{2-3}$$

where

$g(K_t, m)$ = the incremental relationships between $K_n/\tau(z)$ for each month (m) and each 0.10 segment of K_t .

The function $y(K_t, \chi)$, where χ is the output of a random number generator, produces a random statistical distribution that matches the observed distribution of K_n at each 0.10 segment of K_t . The function $\tau(z)$ is defined by

$$\tau(z) = 0.8847 \exp(-0.106h \sec z) , \tag{2-4}$$

where $h = 1$ for altitudes less than 1150 ft and $h = p^2$ for altitudes greater than 1150 ft, where p is the station pressure in atmospheres. Introducing the term $\tau(z)$ provides a correction for variations in zenith angle or air mass.

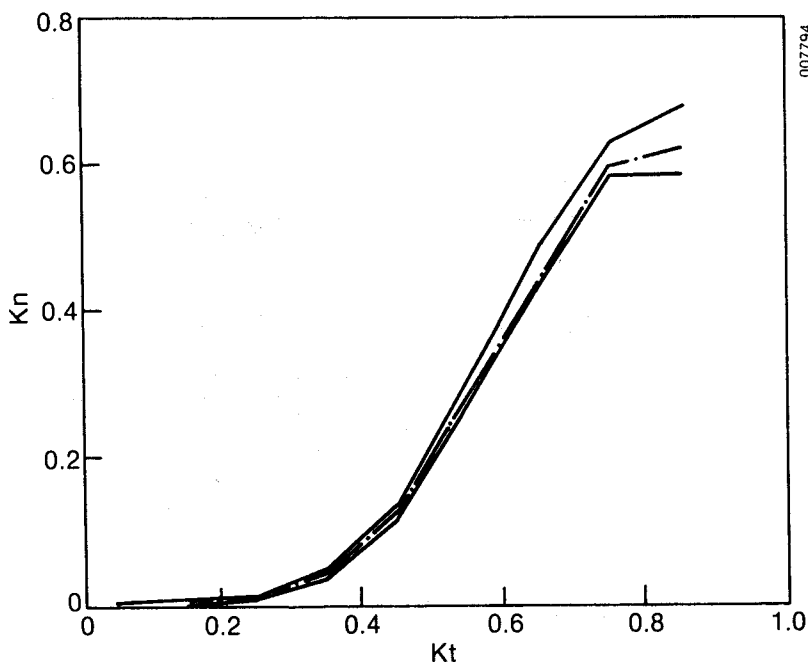


Figure 2-2. Five Station Means and Station Extreme Values of the Segmented Relationship between K_n and K_t (all months)
Source: Randall and Whitson 1977.

NOAA used the ADIPA model to generate 23 years of direct normal data for each of the 26 SOLMET sites. For Ersatz sites, however, direct normal values were computed only for a typical meteorological year (TMY). The ADIPA algorithm was simplified by eliminating the stochastic $y(K_t)$ term, which also necessitated some modification in the incremental relationships for high K_t values. This modified algorithm is called the ETMY model.

2.1.2 Performance of the ADIPA and ETMY Models

In general, these models underestimate direct normal irradiance under clear-sky conditions and overestimate under partially cloudy conditions. Thus, for three stations in the Southwest (Albuquerque, Barstow, and China Lake), a comparison of calculated minus observed monthly mean daily totals yielded negative results (mean difference of -11%) for 45 out of 46 station-months (Hall et al. 1980). In contrast, similar comparisons for data from Toronto and Vancouver, Canada, exhibited a positive difference (mean difference of 7.6%) for 20 out of 29 station-months. Bird obtained similar results (1985) in evaluating the ADIPA and ETMY models with data obtained by West Associates in the southwestern United States, by Georgia Institute of Technology (GIT) in Atlanta, and by the State University of New York in Albany.

Randall (1986) compared the modeled SOLMET and Ersatz direct normal data with 1 to 3 years of measured data from the new NOAA network. He found a mean difference of 14.2% between the new NOAA network measurements and SOLMET modeled data. Of the 179 station-months considered, 68% had differences between -10.2% and 41.6%. If these differences were normally distributed, the results would correspond to a standard deviation of $\pm 26\%$. These differences, however, are large and unacceptable, considering that the data generally represent 3-

to 23-year means of monthly means collected from daily totals. Of course, the SOLMET and new NOAA network data span different time periods, so long-term atmospheric changes could be part of the cause of the mean differences.

Analyses conducted in the Solar Energy Research Institute's (SERI's) current study indicate some of the underlying causes for these large differences. Figure 2-3 includes plots of both the direct normal and global horizontal 1-min data for Albany, N.Y., gathered on April 21, 1979, along with average hourly differences between the measured direct normal data and estimates made using the ETMY model. Figure 2-4 is a similar plot for data from Atlanta, Ga., gathered on June 28, 1981. From the plots of the 1-min data, we know that April 21 was a clear day and June 28 was a partly cloudy day, probably with many scattered clouds causing rapid fluctuations in the intensity of the irradiance. Errors from 10%-50% are indicated on both of the figures. On the clear day, all differences are negative, whereas on the partly cloudy day, the differences are positive until late afternoon, when the sky apparently cleared.

These results explain the tendency of the ADIPA and ETMY models to underestimate for stations and months with a majority of clear days and to overestimate for cloudier climates or months. Apparently the parameter $\tau(z)$ did not adequately account for the effects of air mass. Perhaps, then, τ should also have been a function of K_t .

2.2 Related Research

Extensive research has been conducted to establish the relationships between the direct, diffuse, and total global horizontal radiation components (Liu and Jordan 1960; Bruno 1978; Bugler 1977; Collares-Pereira and Rabl 1979; Iqbal 1980; Orgill and Hollands 1977; Gordon and Hochman 1984; Vignola and McDaniel 1984 and 1986; Garrison 1985; Jeter and Balaras 1985 and 1986). The work of Liu and Jordan (1960) represents a landmark attempt to develop an algorithm for estimating diffuse irradiance from measurements of global horizontal irradiance. Because they had adequate research data from only one location--Hump Mountain, N.C.--they were unable to evaluate the accuracy of their algorithms at other locations. Iqbal's correlations (1980), which he developed with data from Canada and France, did not agree with Liu and Jordan's results. Thus, Iqbal concluded that his correlations, between hourly diffuse radiation and hourly global radiation, might safely be used in the vicinity of the five stations studied. He advised that further work be undertaken when more data become available.

Vignola and McDaniel (1984, 1986) also studied the correlations between direct beam, diffuse horizontal, and global horizontal components. They observed seasonal variations in these correlations and concluded that they were most probably caused by the combined effects of air mass, water vapor, and turbidity. They concluded that, on the average, the beam intensity on individual days can be determined to within 20% of its actual value; however, monthly averages can be determined to within 10%. They did not assess the accuracy of estimating hourly values.

Gordon and Hochman (1984) also studied the correlations between direct beam and total radiation using data collected in Beth Dagan, Israel. Like other researchers in this work, they limited their evaluations to a study of the relationships between the direct beam (K_n) and global horizontal (K_t)

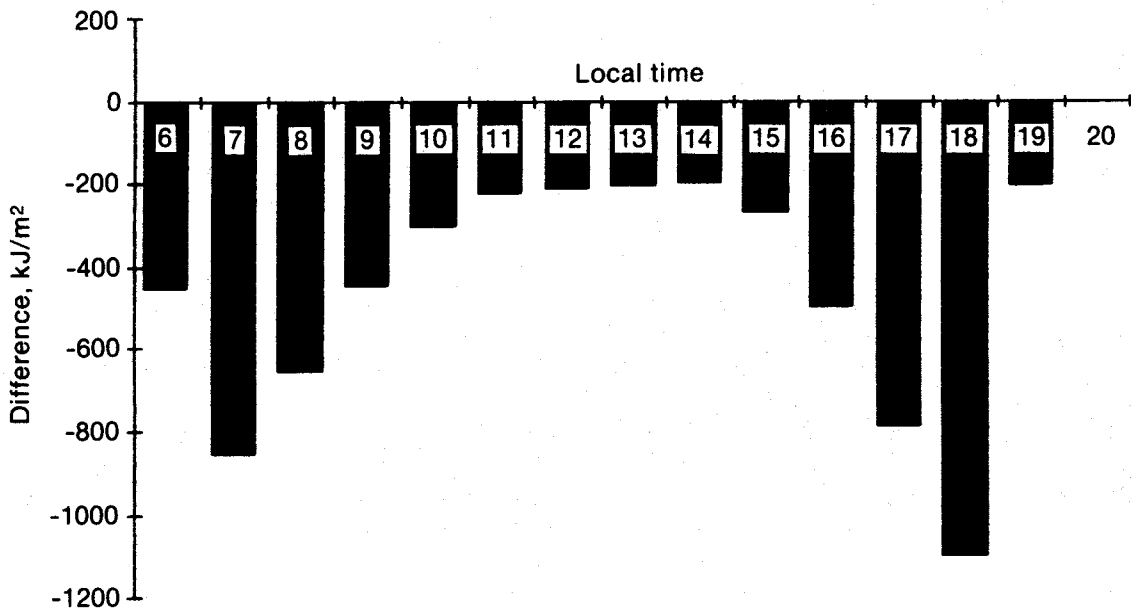
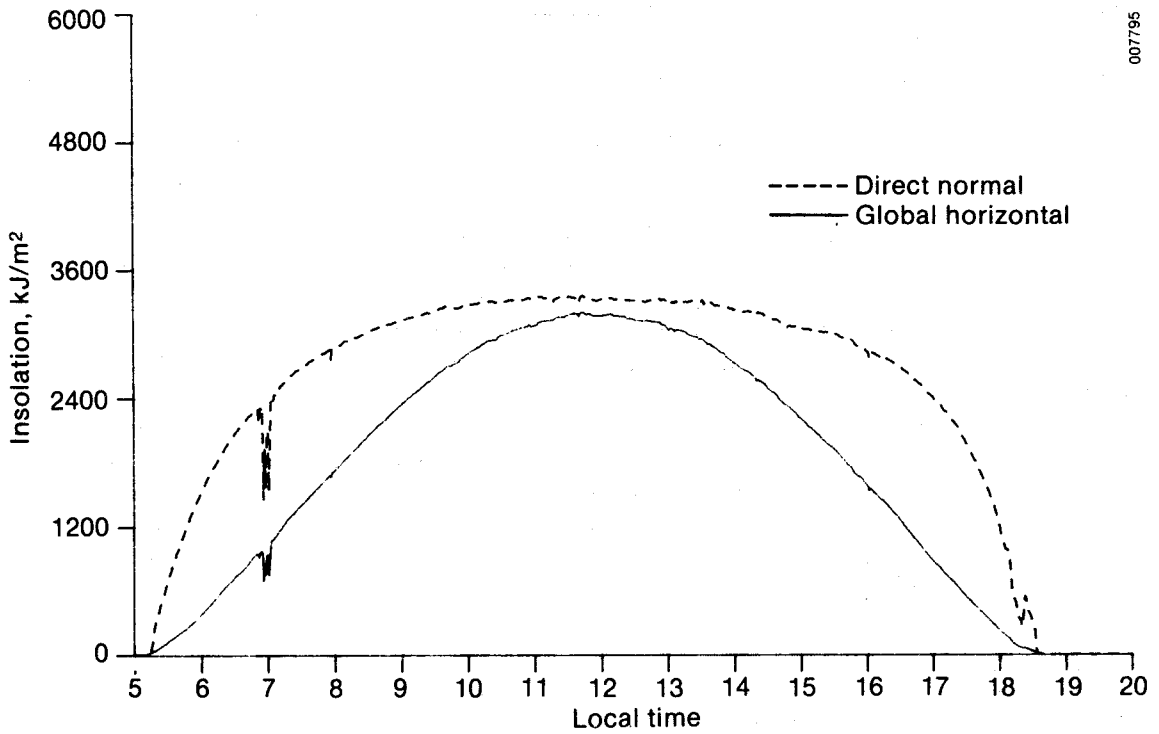


Figure 2-3. One-Minute Data and ETMY (Modeled Minus Observed) Differences for Hourly Means of Direct Normal Insolation for Albany, N.Y., on April 21, 1979

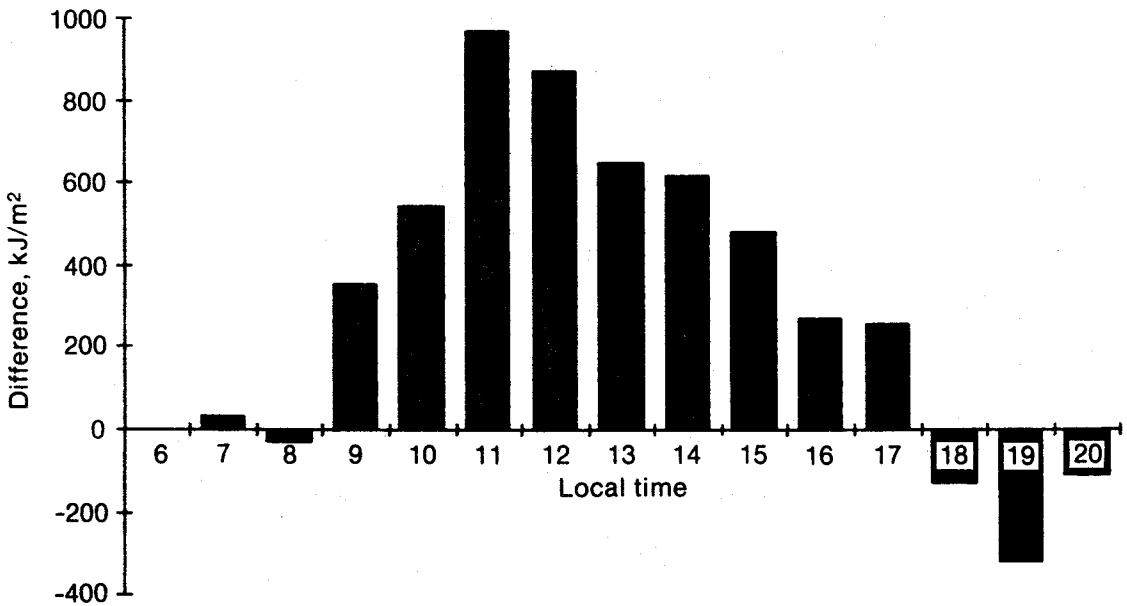
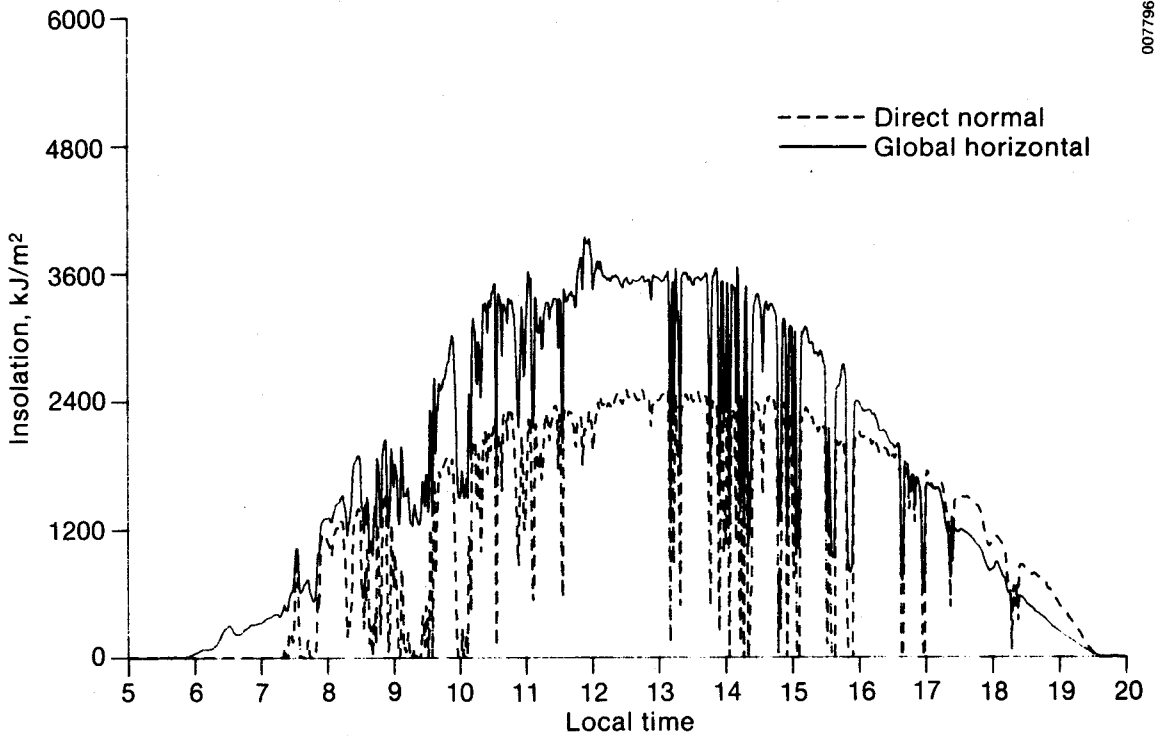


Figure 2-4. One-Minute Data and ETMY (Modeled Minus Observed) Differences for Hourly Means of Direct Normal Insolation for Atlanta, Ga., on June 28, 1981

transmittance values, as defined previously. They found "fairly broad distributions of K_n about a given K_t , and of K_t about a given K_n ."

Garrison (1985) studied the division of total radiation into direct beam and diffuse components at 33 U.S. sites, using data from the new NOAA network. No studies before Garrison's investigated the dependence of the direct and diffuse components with respect to so many different variables. Figures 2-5 and 2-6 exemplify the results of Garrison's research, showing the extreme differences in the diffuse horizontal transmittance found on a turbid, humid summer day compared with that of a clear, dry winter day with a high surface albedo. Diffuse horizontal transmittance (K_d) is defined by

$$K_d = I_d / I_o \cos z , \tag{2-5}$$

where

I_d = diffuse horizontal irradiance at the earth's surface.

Intermediate conditions produce large fluctuations in the relationship between these two variables. Garrison's results provided a clear direction for the research described in this report.

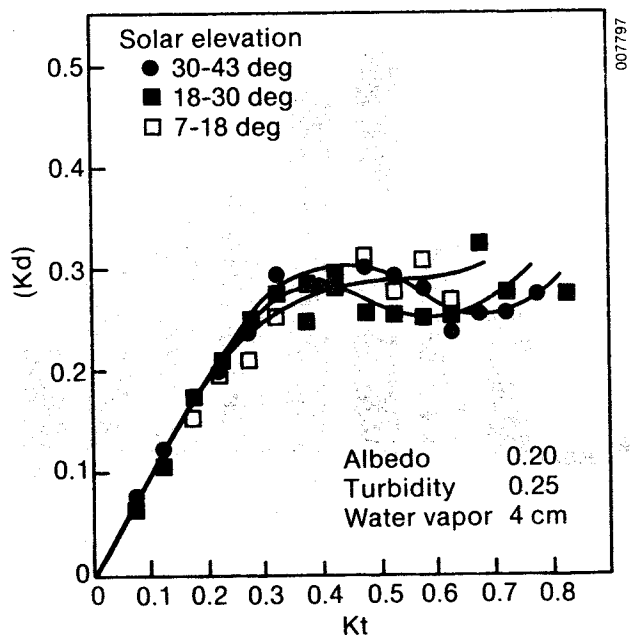


Figure 2-5. Mean K_d Values vs. K_t for Summer Conditions (Data from 33 stations of the new NOAA network)

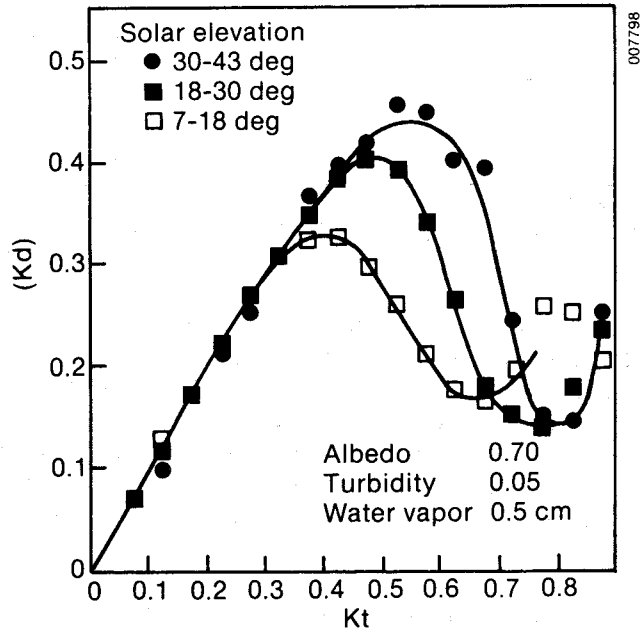


Figure 2-6. Mean Kd Values vs. Kt for Winter Conditions (Data from 33 stations of the new NOAA network)

Using 5 years of data collected at the Shenandoah Solar Total Energy Project (STEP) site in Shenandoah, Ga., Jeter and Balaras (1986 and 1987) developed a seasonal regression model for the beam transmittance of the atmosphere, that is very similar to the ADIPA and ETMY models. While developing these models, Jeter and Balaras noted significant variations in the relationship between K_n and K_t from year to year as well as from season to season within each year. As an alternative to monthly regression coefficients, Jeter and Balaras applied a simple multiplicative seasonal correction factor for each month. Their results indicate that the year-to-year variations can be as great as the variations within a single year. Therefore, the feasibility of using a simple regression model, like the ADIPA and ETMY models, in estimating direct normal data from global horizontal measurements is uncertain.

3.0 DEVELOPMENT OF THE MODEL

The research referred to in Section 2.0 and the physical processes occurring in the atmosphere clearly indicate that the relationship between K_n and K_t is a function of air mass, cloud cover, precipitable water vapor, atmospheric turbidity, and albedo. However, it was uncertain whether a model can be developed for estimating direct normal insolation from global horizontal measurements that would make effective use of these parametric relationships. Ideally, the model should account for parametric effects intrinsically, without requiring input data for the parameters themselves.

GIT provided a 1-year data set of hourly values for all pertinent variables. The cloud-cover and precipitable water vapor data were obtained from the National Weather Service at the Atlanta airport, about 20 miles from the GIT solar radiation measurement site. Apparently this spatial separation did not destroy the relationships between these and other variables, although it undoubtedly had some effect. This data set offered a unique opportunity to investigate the interrelationships between the variables of interest.

We developed the DISC model using a series of sequential steps that ultimately produced the algorithms that formed the model. In the first step, we verified the significance of seasonal, annual, and climate variations in the relationships between K_n and K_t . During the next step, we looked for details to clarify the effect of the parametric variables on the relationships between K_n and K_t . We accomplished this step through multiple correlation studies and through various parametric studies whereby we fixed one or two variables within narrow ranges while we varied the others. In the final step, we developed the algorithms themselves. This step was guided by the results of the preceding analyses and also involved a sequential process.

From the start, we believed that the best method for developing this model was to incorporate parametric variables by relating them to discrete changes in atmospheric transmittances (i.e., ΔK_t and ΔK_n) rather than to the magnitude of atmospheric transmittances. We felt that individual simple functions might be found to compute the change in K_n relative to each parameter (air mass, cloud cover, water vapor, and so on) for selected ranges of K_t . Furthermore, the effect of the various parametric variables on ΔK_n might be similar for a given K_t , leading to a simple model that would account intrinsically for the effect of the parametric variables. Hence, these new ΔK variables were included in the analyses.

3.1 Direct Normal versus Global Horizontal Relationships

3.1.1 Seasonal, Annual, and Climate Relations

Before examining the variables affecting the K_n versus K_t relationships, we evaluated seasonal, annual, and climate variations to verify and extend the previous work of others. A third-order polynomial regression equation was fit to seasonal data sets for six stations, using up to 3 years of data.

Typical seasonal variations are illustrated in Figure 3-1, using data from Atlanta for the years 1980 to 1982. These results are consistent with the climate at Atlanta, which generally exhibits high water vapor and cloud cover

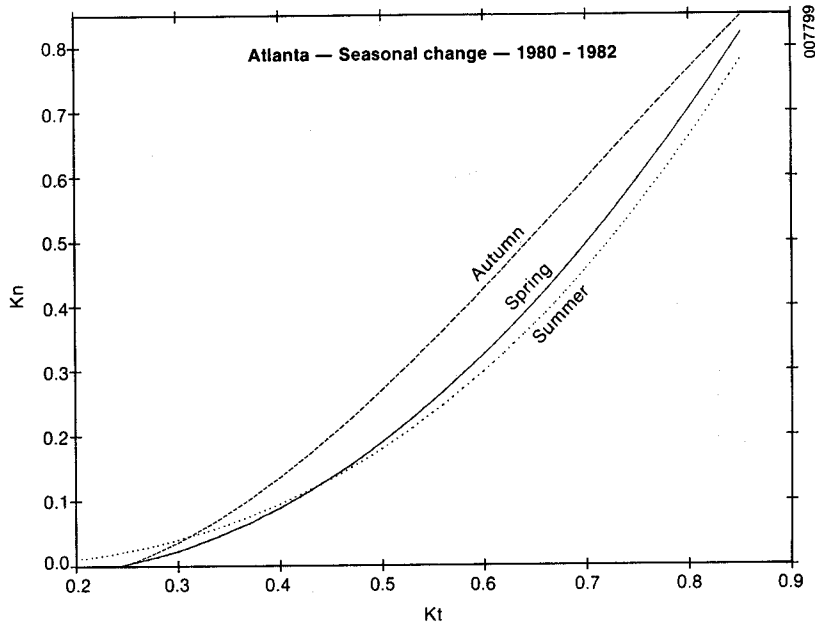


Figure 3-1. Observed Seasonal Changes in the Relationship between K_n and K_t (Third-order regression fits to three years of data from Atlanta, Ga.)

during the summer months. The clearest parts of the year are normally the late fall and early winter months.

Annual variations are illustrated in Figure 3-2, with data obtained during the spring in Las Vegas, Nev. The annual variations, of course, are random; for some stations and seasons, we noted virtually no change from year to year. Nevertheless, using a single regression equation to relate K_n and K_t will obviously result in changes in the accuracy of these estimations from year to year.

Climate changes are indicated in Figure 3-3, which shows the regression relationships obtained during the summer for all six data sets employed in this part of our study. Using a single regression relationship between K_n and K_t apparently will not work well at all stations or at a given station for all seasons. These results confirmed and supplemented the results referred to earlier.

3.1.2 Multiple Correlation Studies

Using the special data set from Atlanta, Ga., we performed multiple correlation analyses using various groupings of the data to gain further insight into the parameters that might cause seasonal, annual, and climate variations. Realizing that solar irradiance is a function of solar elevation or air mass, the data were grouped into solar elevation bins to minimize the effect of air mass on the multivariate correlations. Although turbidity data are a part of this data set, they were not included in some of these analyses because of the sparsity of data and because of our concern that including turbidity would bias the resulting data set toward those conditions that favored turbidity

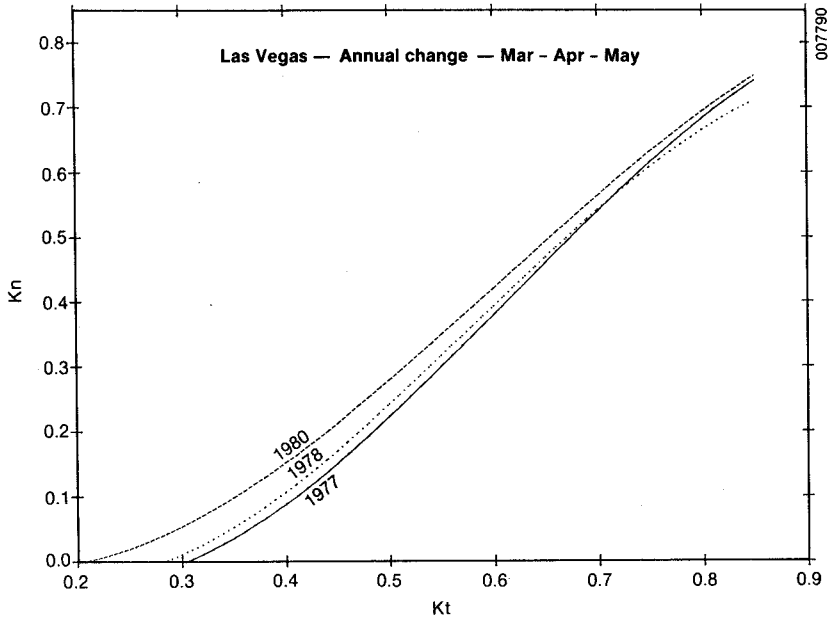


Figure 3-2. Observed Annual Changes in the Relationship between K_n and K_t (Third-order regression fits to data for March, April, and May from Las Vegas, Nev.)

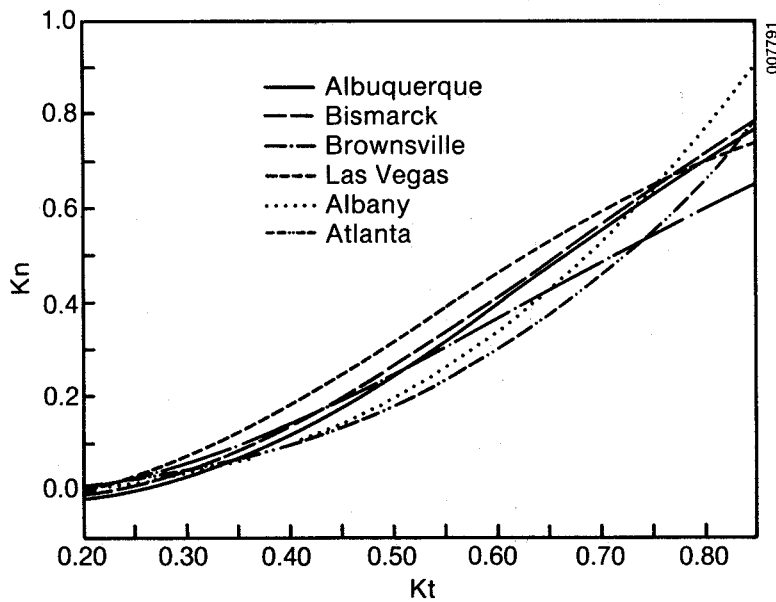


Figure 3-3. Observed Differences in the Relationship between K_n and K_t Possibly Caused by Climate Differences [Third order regression fits to three years of summer (July and August) data for the six locations indicated.]

measurements. These correlations are based on hourly data; samples for shorter or longer periods are likely to exhibit different correlations.

The correlation matrices shown in Table 3-1 are quite informative. For example, diffuse irradiance shows no apparent correlations with any of the variables, except for the correlation with global irradiance for the 5- to 15-deg solar elevation range. From this result, one might suspect that the range of diffuse values in the October 1981 data from Atlanta was quite limited. However, the statistics from this period, given in Table 3-2, show that this was not the case. The data appear to represent a wide range of atmospheric conditions. Therefore, diffuse irradiance may be primarily a function of turbidity and perhaps air mass, since variations in air mass are quite limited within each solar elevation range. However, the actual relationship between global and diffuse irradiance is nonlinear and is, therefore, misrepresented by a linear correlation analysis (see Section 3.1.3).

The information in Table 3-1 shows that the correlations between radiation components and between each component and other variables, such as total and opaque cloud cover, tend to increase with increasing solar elevation. Furthermore, with only one exception, opaque cloud cover is more closely correlated with direct and global irradiance than is total cloud cover. Also, the higher correlation between global and direct irradiance and percent sunshine, compared with the correlation between global and direct irradiance and cloud cover, is misleading, because the percent sunshine data were derived from the direct normal data, and the cloud-cover observations were made at the Atlanta airport, about 20 miles from GIT. In general, precipitable water vapor and visibility show only moderate correlations with solar irradiance values.

We formed a subset of the October 1981 data from Atlanta by selecting those hours for which total cloud cover was less than 10%. With this subset, which favors turbidity measurements, the turbidity at 500 nm was included in the correlation analyses (Table 3-3). Under these conditions, one finds that diffuse irradiance is highly correlated with turbidity, whereas global horizontal and direct normal irradiance are not. Furthermore, diffuse irradiance now shows a significant correlation with precipitable water vapor, whereas the correlation with precipitable water vapor was very poor for the data sets grouped according to solar elevation. Under these conditions, precipitable water vapor and turbidity show a correlation of 0.83.

3.1.3 Parametric Studies

Because of these results and the results of other researchers, and recognizing the sparsity of turbidity data, we decided to limit the parameters to be studied to K_t (derived from global horizontal data), air mass, cloud cover, and precipitable water vapor. To isolate the effect of one variable from another, new subsets of the Atlanta 1981 data were formed. Table 3-4 shows the ranges used to form data sets grouped according to air mass, cloud cover, and precipitable water vapor. Selected ranges for two of these three variables were used to form each subset. For each subset, plots of K_t versus K_n and K_d were made as well as plots of ΔK_t vs. ΔK_n . The latter variables are defined as

Table 3-1. Multiple Correlations for Hourly Atlanta Data Grouped by Solar Elevation (October 1981)

	DIRN	GLOB	DIF	SS%	H ₂ O	VIS	Kt	TOTCLD	OPQCLD ^a
Elevation = 5 to 15 deg									
DIRN	2	1.0000							
GLOB	3	0.8449	1.0000						
DOF	4	0.2745	0.6914	1.0000					
SS%	5	0.9862	0.8221	0.2701	1.0000				
H ₂ O	6	-0.4621	-0.4376	-0.2618	-0.4239	1.0000			
VIS	7	0.4740	0.3425	0.1576	0.4888	-0.6633	1.0000		
AKt	8	0.8628	0.8785	0.5883	0.8650	-0.6031	0.5136	1.0000	
TOTCLD	9	-0.7921	-0.5673	-0.0893	-0.7963	0.4106	-0.4099	-0.7436	1.0000
OPQCLD	10	-0.7648	-0.5960	-0.2549	-0.7855	0.4990	-0.5452	-0.8197	0.9095 1.0000
Elevation = 15 to 25 deg									
DIRN	2	1.0000							
GLOB	3	0.8896	1.0000						
DIF	4	-0.2266	0.2233	1.0000					
SS%	5	0.9699	0.9107	-0.1316	1.0000				
H ₂ O	6	-0.5319	-0.5867	-0.1718	-0.4658	1.0000			
VIS	7	0.4128	0.4701	0.1993	0.3910	-0.6447	1.0000		
AKt	8	0.8981	0.9801	0.2079	0.9075	-0.6409	0.5559	1.0000	
TOTCLD	9	-0.8224	-0.7151	0.1686	-0.7664	0.4393	-0.4318	-0.7558	1.0000
OPQCLD	10	-0.8617	-0.8035	0.0853	-0.8527	0.4944	-0.5150	-0.8353	0.9334 1.0000
Elevation = 25 to 35 deg									
DIRN	2	1.0000							
GLOB	3	0.9090	1.0000						
DIF	4	-0.3943	0.0101	1.0000					
SS%	5	0.9798	0.9204	-0.3148	1.0000				
H ₂ O	6	-0.5017	-0.5980	-0.1568	-0.4635	1.0000			
VIS	7	0.3744	0.4986	0.2428	0.3633	-0.5781	1.0000		
AKt	8	0.9164	0.9860	-0.0012	0.9312	-0.6294	0.5217	1.0000	
TOTCLD	9	-0.8675	-0.7823	0.3272	-0.8392	0.4474	-0.3574	-0.8030	1.0000
OPQCLD	10	-0.8966	-0.8477	0.2707	-0.8892	0.4827	-0.4515	-0.8565	0.9552 1.0000

^aDIRN = direct irradiance
 GLOB = global irradiance
 DIF = diffuse irradiance
 SS% = percent sunshine
 H₂O = precipitable water vapor

VIS = visibility
 Kt = global horizontal transmittance
 TOTCLD = total cloud cover
 OPQCLD = opaque cloud cover

Table 3-1. Multiple Correlations for Hourly Atlanta Data Grouped by Solar Elevation (October 1981) (Concluded)

	DIRN	GLOB	DIF	SS%	H ₂ O	VIS	Kt	TOTCLD	OPQCLD ^a	
Elevation = 35 to 45 deg										
DIRN	2	1.0000								
GLOB	3	0.9136	1.0000							
DIF	4	-0.4483	-0.0546	1.0000						
SS%	5	0.9801	0.9345	-0.3463	1.0000					
H ₂ O	6	-0.5919	-0.6804	-0.0308	-0.5420	1.0000				
VIS	7	0.4350	0.5306	0.0784	0.4312	-0.5782	1.0000			
AKt	8	0.9163	0.9939	-0.0556	0.9385	-0.6877	0.5301	1.0000		
TOTCLD	9	-0.8588	-0.7541	0.4518	-0.8277	0.4829	-0.4063	-0.7574	1.0000	
OPQCLD	10	-0.9191	-0.8286	0.4415	-0.9023	0.4952	-0.4684	-0.8288	0.9526	1.0000

Elevation = 45 to 55 deg

DIRN	2	1.0000								
GLOB	3	0.9550	1.0000							
DIF	4	-0.3604	-0.0742	1.0000						
SS%	5	0.9769	0.9722	-0.2174	1.0000					
H ₂ O	6	-0.6085	-0.6009	0.1549	-0.5386	1.0000				
VIS	7	0.6562	0.7043	-0.0292	0.6212	-0.6898	1.0000			
AKt	8	0.9540	0.9975	-0.0654	0.9748	-0.6052	0.6943	1.0000		
TOTCLD	9	-0.7814	-0.7460	0.2714	-0.7684	0.4108	-0.3198	-0.7468	1.0000	
OPQCLD	10	-0.9333	-0.9006	0.3016	-0.9382	0.4728	-0.5119	-0.8976	0.8788	1.0000

^aDIRN = direct irradiance

GLOB = global irradiance

DIF = diffuse irradiance

SS% = percent sunshine

 H₂O = precipitable water vapor

VIS = visibility

Kt = global horizontal transmittance

TOTCLD = total cloud cover

OPQCLD = opaque cloud cover

**Table 3-2. Statistics for Atlanta Data
(October 1981)**

Variable	Mean	Standard Deviation	Min.	Max.
I_n	1352	1311	2.4	3617
I_t	1162	900	10.7	3089
I_d	405	298	21.7	1385
%SS	52	46	0.2	100
H_2O	1.98	0.78	0.50	3.80
$\tau(500)^a$	0.24	0.10	0.06	0.59
VIS	23.20	14.66	0.00	72.40
Kt	0.44	0.25	0.01	0.79
TOTCLD	6.16	3.86	0.00	10.00
OPQCLD	5.22	4.19	0.00	10.00

^aTurbidity values for partial data set for cloud-cover less than 10%.

**Table 3-3. Multiple Correlations of Atlanta Data with Less Than 10%
Cloud Cover (October 1981)**

	DIRN	GLOB	DIF	TURB5	H_2O	VIS	Kt ^a
DIRN	1	1.0000					
GLOB	3	0.8199	1.0000				
DIF	5	-0.0347	0.4541	1.0000			
TURB5	8	-0.3268	0.1896	0.9002	1.0000		
H_2O	9	-0.4772	-0.0010	0.7907	0.8325	1.0000	
VIS	10	0.4414	0.0804	-0.5334	-0.6829	-0.7512	1.00
AKt	11	0.9729	0.9040	0.1799	-0.1283	-0.3009	0.33 1.00

^aDIRN = direct irradiance

GLOB = global irradiance

DIF = diffuse

TURB5 = turbidity at 500 nm

H_2O = precipitable water vapor

VIS = visibility

Kt = global horizontal transmittance

Table 3-4. Variable Ranges Used To Form Data Subsets

Legend	Name	Range
LAM	Low air mass	$1.0 \leq AM \leq 1.11$
MAM	Medium air mass	$4.0 \leq AM \leq 6.0$
HAM	High air mass	$6.0 \leq AM \leq 18.0$
LCC	Low cloud cover	$0.0 \leq OPQCC \leq 0.2$
MCC	Medium cloud cover	$0.3 \leq OPQCC \leq 0.6$
HCC	High cloud cover	$0.7 \leq OPQCC \leq 1.0$
LH ₂ O	Low water vapor	$0.0 \leq H_2O \leq 1.5 \text{ (cm)}$
HH ₂ O	High water vapor	$3.0 \leq H_2O \leq 6.0$

$$\Delta Kt = Kt_c - Kt, \quad (3-1)$$

and

$$\Delta Kn = Kn_c - Kn, \quad (3-2)$$

where Kt_c and Kn_c are limiting values for global and direct normal transmittance under clear-sky conditions (as observed at Atlanta, Ga.), and Kt and Kn are calculated values for individual hourly data points.

Figure 3-4 is a scatter plot of four of the data subsets defined in Table 3-4. As might be expected, the low-air-mass/low-cloud-cover (LAM-LCC) subset shows the highest Kt and Kn values. The low-air-mass/medium-cloud-cover (LAM-MCC) data set joins smoothly with the other and appears to approach $Kn = 0$ exponentially. The medium-air-mass/low-cloud-cover (MAM-LCC) and medium-air-mass/high-cloud-cover (MAM-HCC) data sets are displaced vertically from the other two, indicating an air mass effect. To show the effects of air mass and cloud cover clearly, only these four subsets were selected for this figure. These examples make it graphically clear that the relationships between Kn and Kt are closely correlated with air mass and cloud cover.

Knowing that previous models relating Kn and Kt , such as the ADIPA and ETMY models, used a single relationship fit to the full scatter of data (such as that shown in Figure 2-1), we can understand why large differences occurred between measured and calculated direct normal values.

A plot of ΔKn versus ΔKt , representing changes from clear-dry conditions, is shown in Figure 3-5 for four combinations of air-mass and cloud-cover ranges. Again, a distinct separation of the data is noted for the two air-mass ranges, and the asymptotic effect of high cloud cover is also apparent.

Figures 3-6 and 3-7 further illustrate the factors affecting the relationship between Kn and Kt . Both are for medium-air-mass (MAM) ranges, but Figure 3-6 represents low-cloud-cover (LCC) conditions and Figure 3-7 illustrates low-precipitable-water-vapor (LH₂O) conditions. These two subsets of data would almost exactly overlap one another if plotted on the same figure. In fact, many of the data points are identical, particularly at high Kt values. These and similar results for other air mass, cloud-cover, and precipitable-water-vapor ranges indicate that using cloud-cover data to modify equations relating

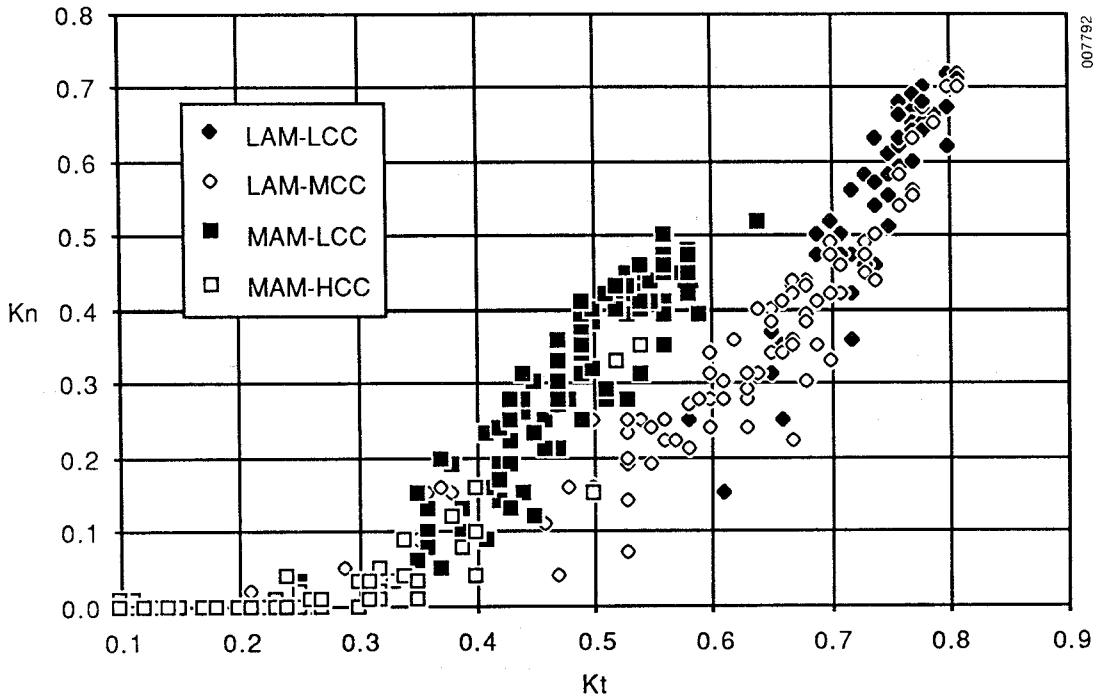


Figure 3-4. Scatter Plots of K_n vs. K_t for Four Subsets of Data from Atlanta, Ga. (October 1981)

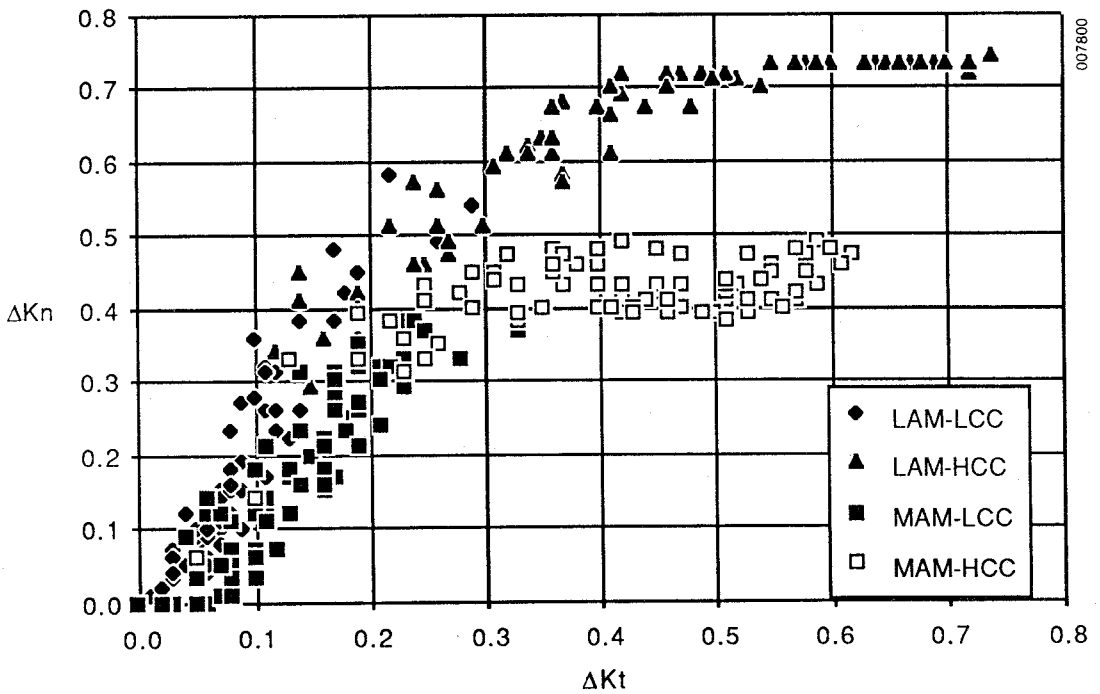


Figure 3-5. Scatter Plots of ΔK_n vs. ΔK_t for Four Subsets of Data from Atlanta, Ga. (October 1981)

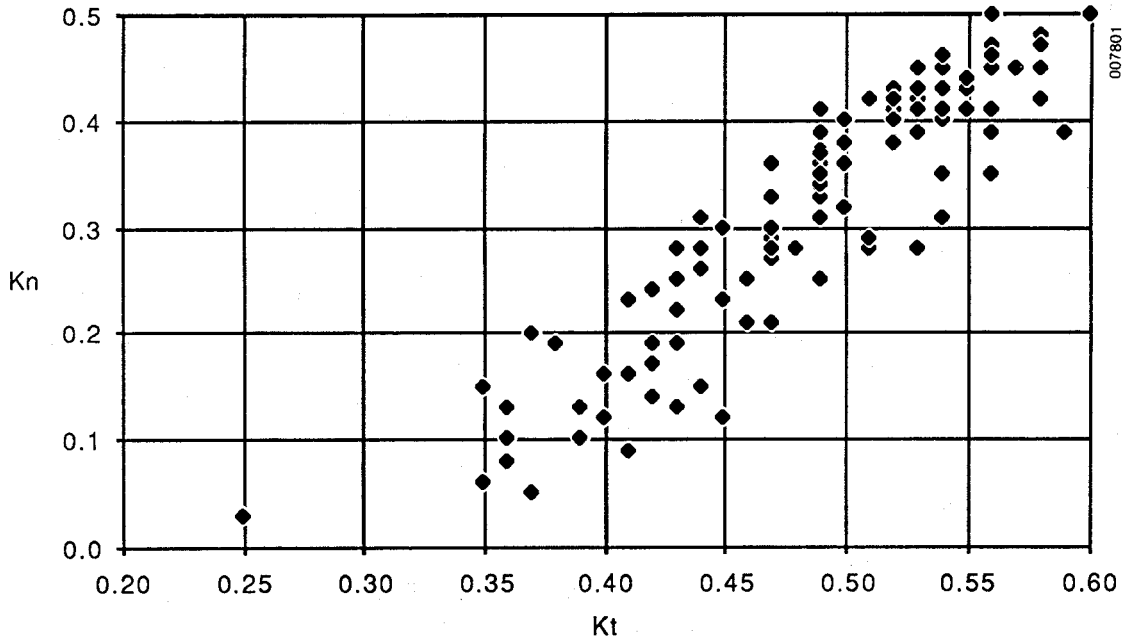


Figure 3-6. Scatter Plot of Kn vs. Kt for Medium Air Mass (4.0 to 6.0) and Low Cloud Cover (0 to 0.2) for Data from Atlanta, Ga. (October 1981)

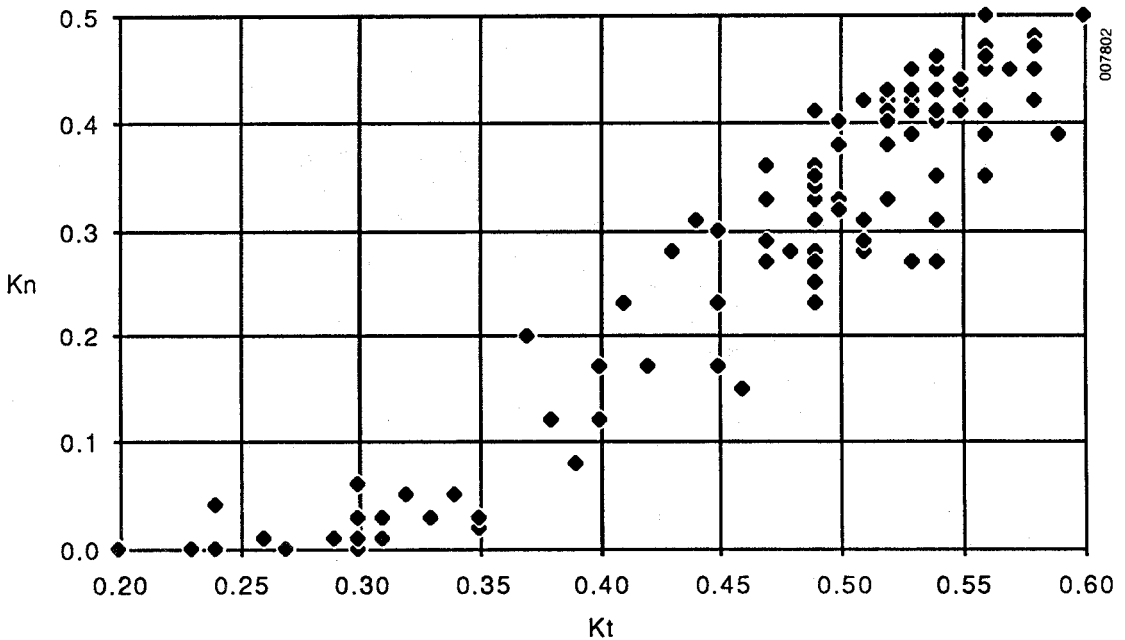


Figure 3-7. Scatter Plot of Kn vs. Kt for Medium Air Mass (4.0 to 6.0) and Low Precipitable Water Vapor (0.0 to 1.5 cm) for Data from Atlanta, Ga. (October 1981)

K_n and K_t will account for much of the variance attributable to both cloud cover and precipitable water vapor.

Although calculating the diffuse component was not an objective of this task, the relationship between K_d and K_t for low-air-mass/low-precipitable-water (LAM-LH₂O) conditions is shown on Figure 3-8. Garrison's (1985) results for similar conditions have been plotted on the same figure, illustrating close agreement between our results using hourly measurements of precipitable water vapor and Garrison's results using seasonal averages for selected NOAA network stations. A similar comparison for medium-air-mass/high-precipitable-water vapor (MAM-HH₂O) conditions is shown in Figure 3-9. These curvilinear relationships between K_d and K_t would account for the low linear correlation coefficients noted in Table 3-1. In other words, the diffuse component of solar irradiance may be closely related to the direct and global components, but in general, this relationship is not linear.

3.2 Developing the Algorithms

Dozens of plots similar to those shown in Figures 3-4 to 3-9 and numerous statistical analyses were performed and studied. Using all of these preliminary results, we formed certain hypotheses and concepts about the structure of a model used to calculate direct normal values from global horizontal data. The hypotheses which guided the actual development of the model were as follows:

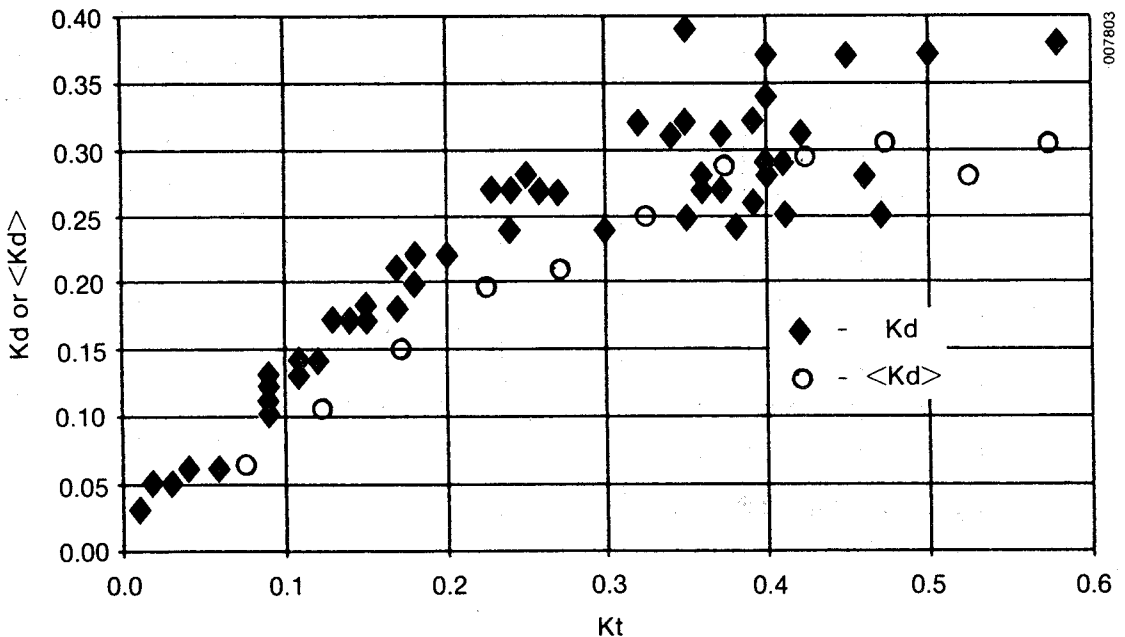


Figure 3-8. Scatter Plots of K_d and $\langle K_d \rangle$ vs. K_t for Similar Hourly and Average Seasonal Conditions, Respectively

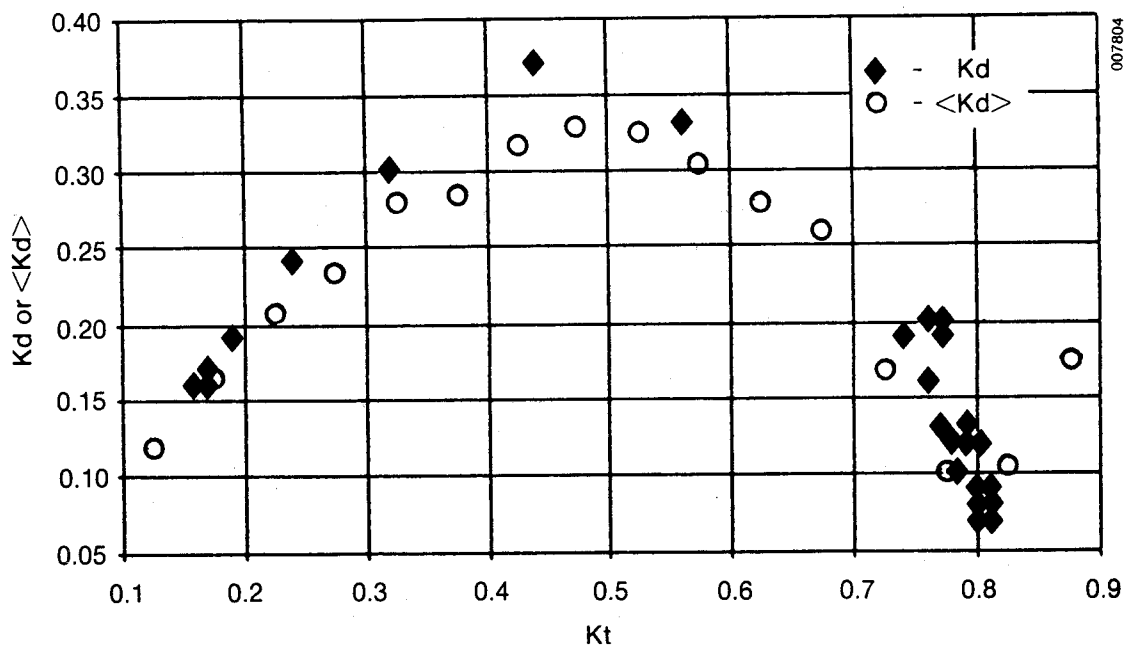


Figure 3-9. Scatter Plot of K_d and $\langle K_d \rangle$ vs. K_t for Similar Hourly and Average Seasonal Conditions, Respectively

- Air mass is the dominant parameter affecting the relationship between K_n and K_t .
- Using a physical model to calculate clear-sky atmospheric transmittance for the direct beam component (K_n) will provide a physically based reference from which changes in K_n (as a function of K_t , air mass, cloud cover, and precipitable water vapor) can be calculated.
- The seasonal, annual, and climate variations in the relationship between K_n and K_t are entirely accounted for by functions parametric in K_t that relate ΔK_n to air mass, cloud cover, and precipitable water vapor.

3.2.1 Establishing Clear-Sky Limits

We used the Bird clear-sky model (Bird and Hulstrom 1981) to calculate a limiting, clear-sky direct beam transmittance (K_{n_c}) as a function of air mass. Based on conditions found in the southwestern United States, the value for precipitable water vapor was set at 0.2 cm and the value for turbidity (at 500 nm) was set at 0.03. These results are shown in Figure 3-10, along with a fourth-order polynomial that was fit to the calculated values. The polynomial represents Bird's clear-sky model for precipitable water vapor of 0.2 cm and turbidity of 0.03. By using a polynomial fit to the results obtained with Bird's model, we greatly simplified the model for calculating direct normal values from global horizontal values.

3.2.2 Deriving the Functional Relationships Between ΔK_n and Air Mass

Since many global horizontal data are not accompanied by concurrent observations of cloud cover and/or measurements of precipitable water vapor, we decided that the initial model would use only global horizontal measurements

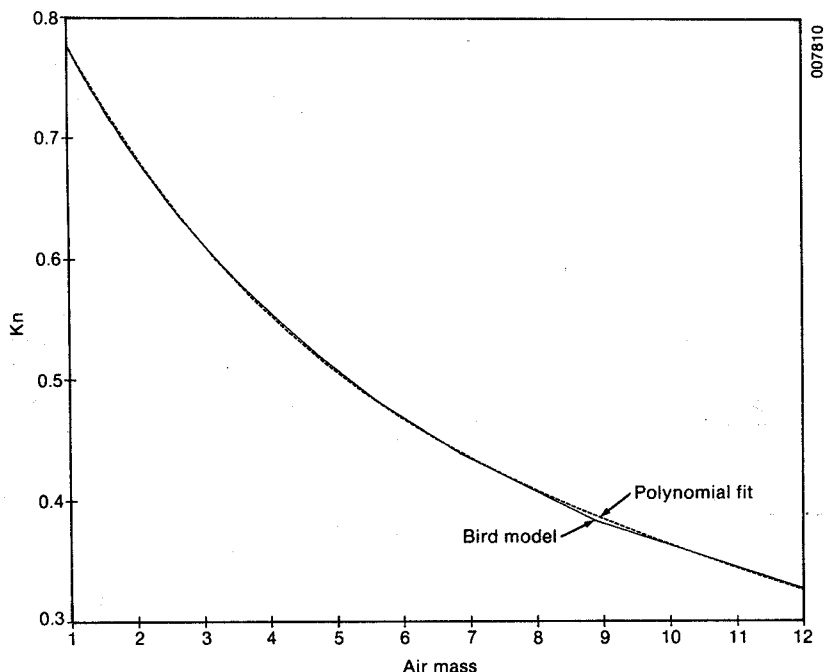


Figure 3-10. K_n vs. Air Mass Calculated for Clear, Dry Conditions (Turbidity = 0.03 and Precipitable Water Vapor = 0.2 cm) Using Bird's Clear-Sky Model

as input data for the calculation of direct normal values. As the next step in developing the model, ΔK_n values were added to the data set for Atlanta, Ga., using Eq. 3-2, and the polynomial

$$K_{nc} = 0.866 - 0.122(AM) + 0.0121(AM)^2 - 0.000653(AM)^3 + 0.000014(AM)^4 \quad (3-3)$$

to fit the clear-sky model values shown in Figure 3-10. Next, subsets of data were formed from the Atlanta data set for K_t ranges from 0.25 to 0.80, in increments of 0.05. For each of these subsets of data, plots of ΔK_n versus air mass were prepared. From these plots, we discovered that a simple exponential relationship existed between air mass and ΔK_n , and a least-squares regression analysis was used to fit each subset of data to the exponential form

$$\Delta K_n = a + b * \exp[c * (AM)] \quad (3-4)$$

The plots of each subset of data and the resultant exponential curves are shown in Figures 3-11(a)-(1).

When the 12 exponential functions were plotted together, we noted an unacceptable irregularity in the curve shapes and their asymptotic values at high air mass. These irregularities were considered unacceptable because physical relationships, such as that between ΔK_n and air mass, usually exhibit smooth, continuous changes over the parametric range of study. Therefore, using the results of the initial functional fits, evenly spaced asymptotic values, represented by coefficient a in Eq. (3-4), were assigned to each of the 12 data sets. Equation (3-4) was again fit to the data, with coefficient a fixed as noted and coefficients b and c established by the least-squares regression

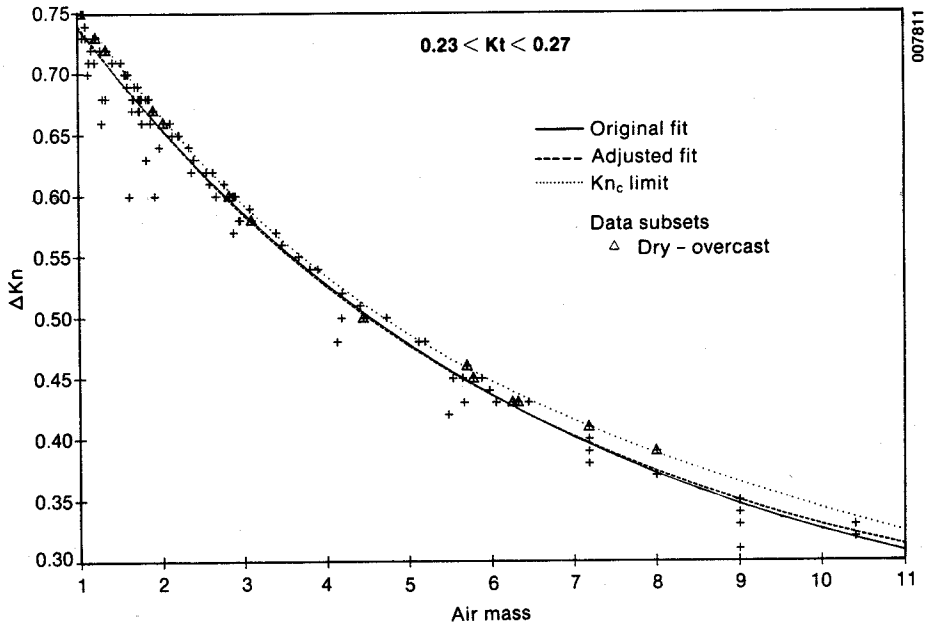


Figure 3-11(a). Scatter Plots of ΔK_n vs. Air Mass and Exponential Fits for an Atlanta Data Subset ($0.23 < K_t < 0.27$) Used in Developing the Algorithms for the DISC Model

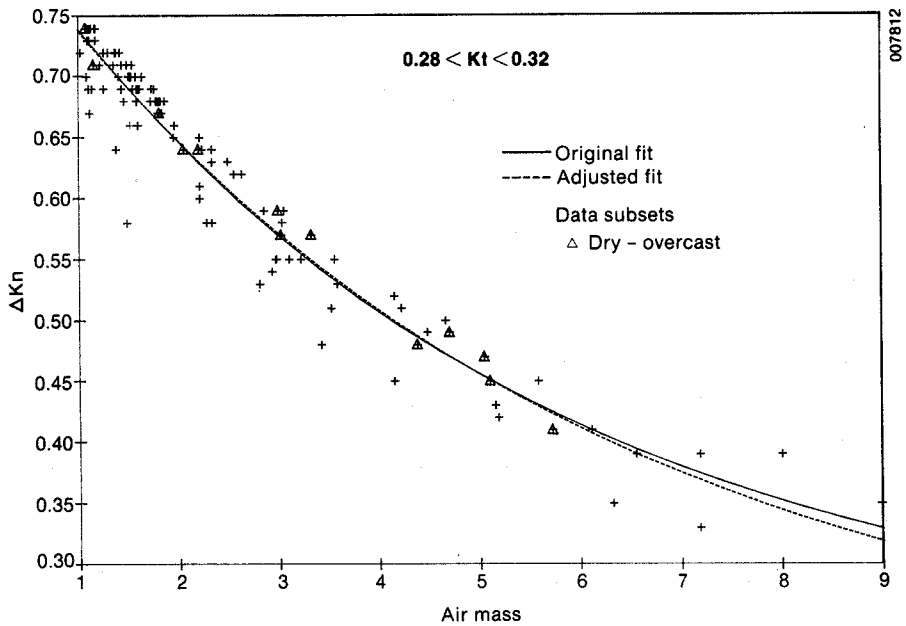


Figure 3-11(b). Scatter Plots of ΔK_n vs. Air Mass and Exponential Fits for an Atlanta Data Subset ($0.28 < K_t < 0.32$) Used in Developing the Algorithms for the DISC Model

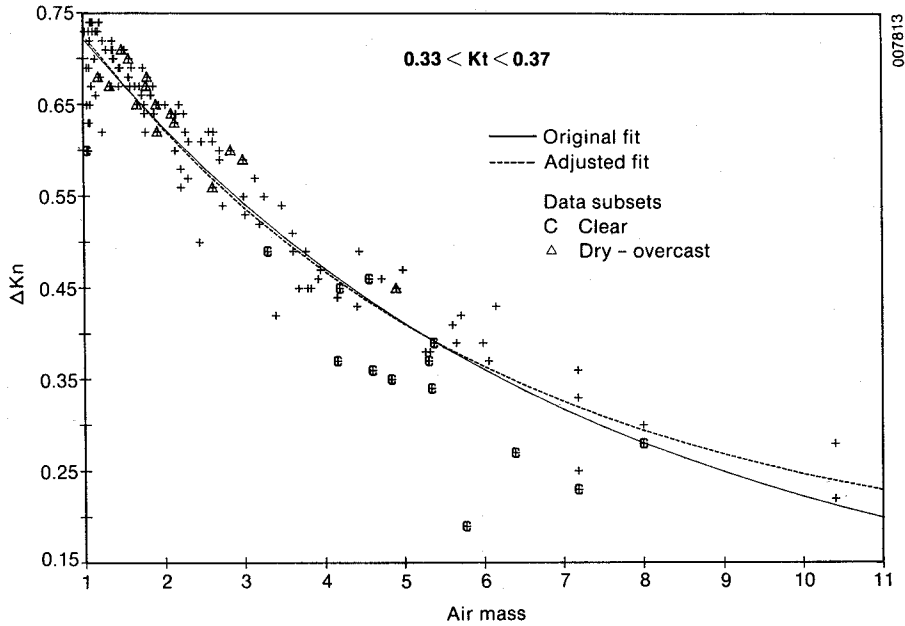


Figure 3-11(c). Scatter Plots of ΔKn vs. Air Mass and Exponential Fits for an Atlanta Data Subset ($0.33 < Kt < 0.37$) Used in Developing the Algorithms for the DISC Model

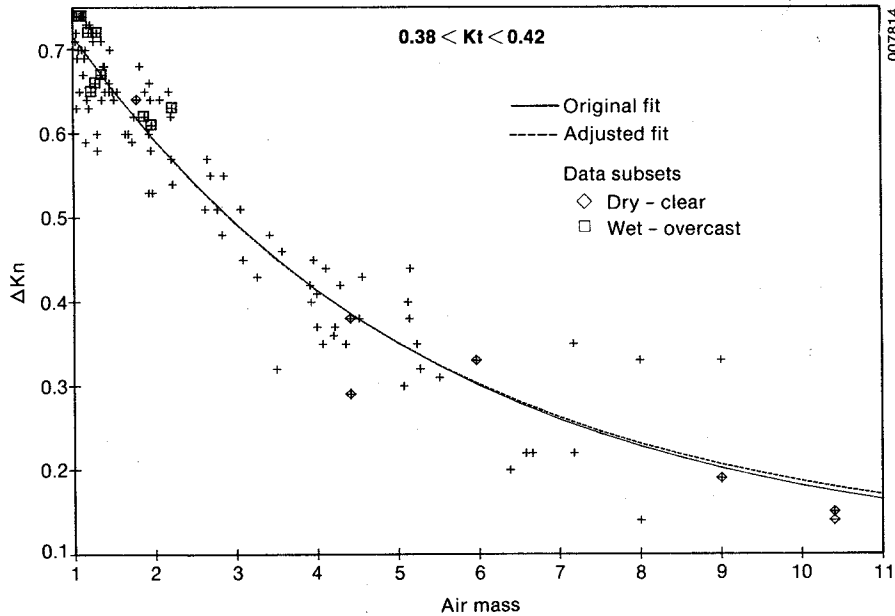


Figure 3-11(d). Scatter Plots of ΔKn vs. Air Mass and Exponential Fits for an Atlanta Data Subset ($0.38 < Kt < 0.42$) Used in Developing the Algorithms for the DISC Model

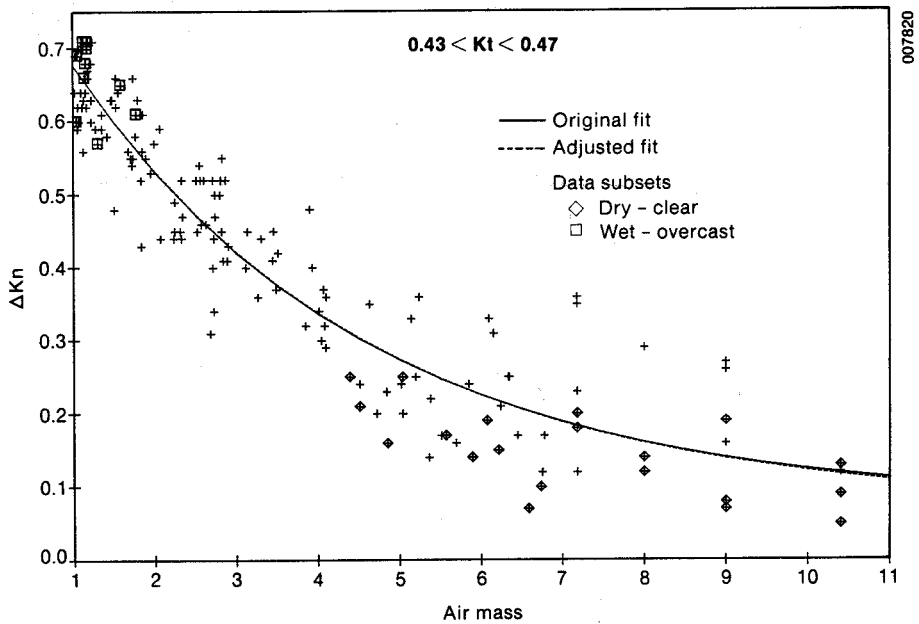


Figure 3-11(e). Scatter Plots of ΔK_n vs. Air Mass and Exponential Fits for an Atlanta Data Subset ($0.43 < K_t < 0.47$) Used in Developing the Algorithms for the DISC Model

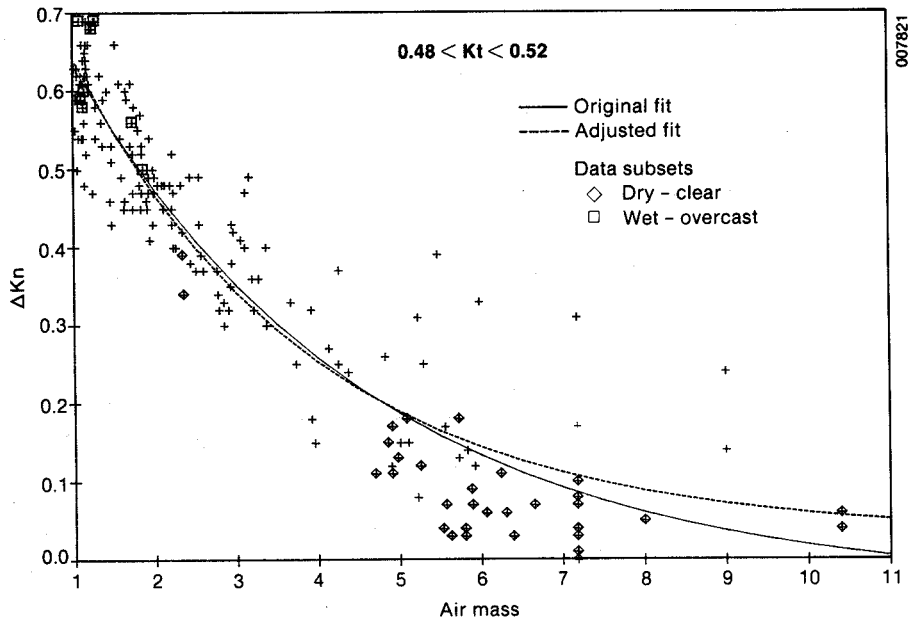


Figure 3-11(f). Scatter Plots of ΔK_n vs. Air Mass and Exponential Fits for an Atlanta Data Subset ($0.48 < K_t < 0.52$) Used in Developing the Algorithms for the DISC Model

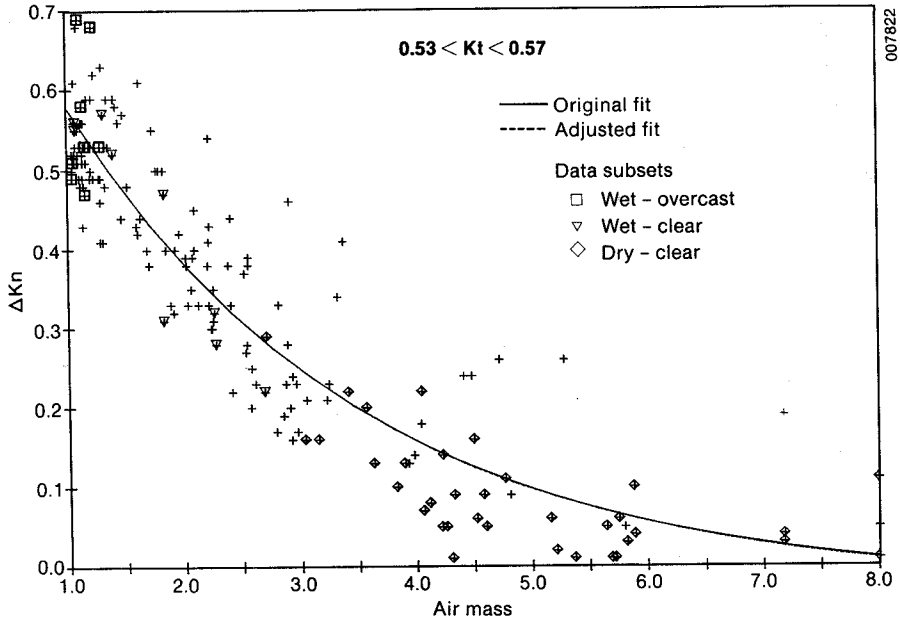


Figure 3-11(g). Scatter Plots of ΔK_n vs. Air Mass and Exponential Fits for an Atlanta Data Subset ($0.53 < K_t < 0.57$) Used in Developing the Algorithms for the DISC Model

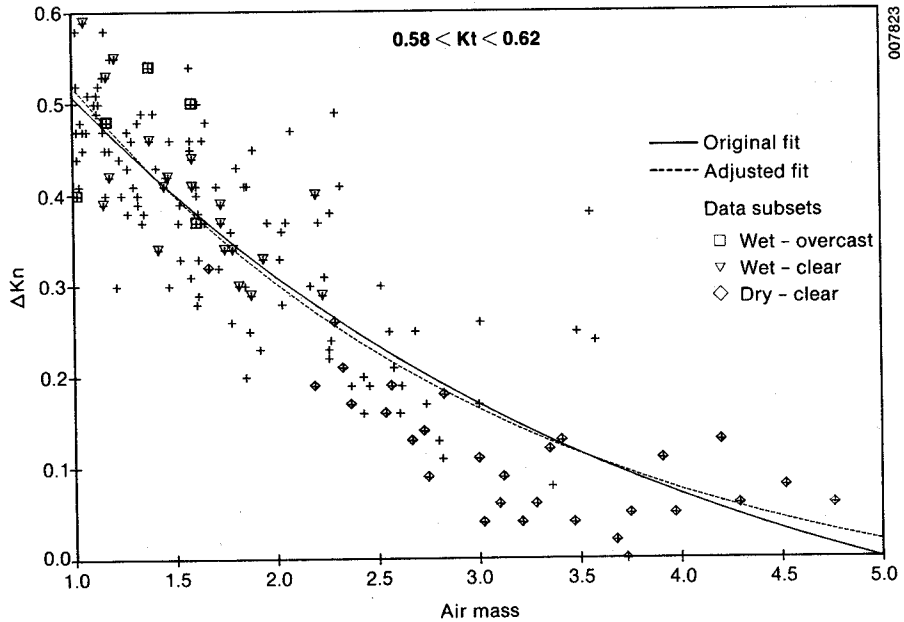


Figure 3-11(h). Scatter Plots of ΔK_n vs. Air Mass and Exponential Fits for an Atlanta Data Subset ($0.58 < K_t < 0.62$) Used in Developing the Algorithms for the DISC Model

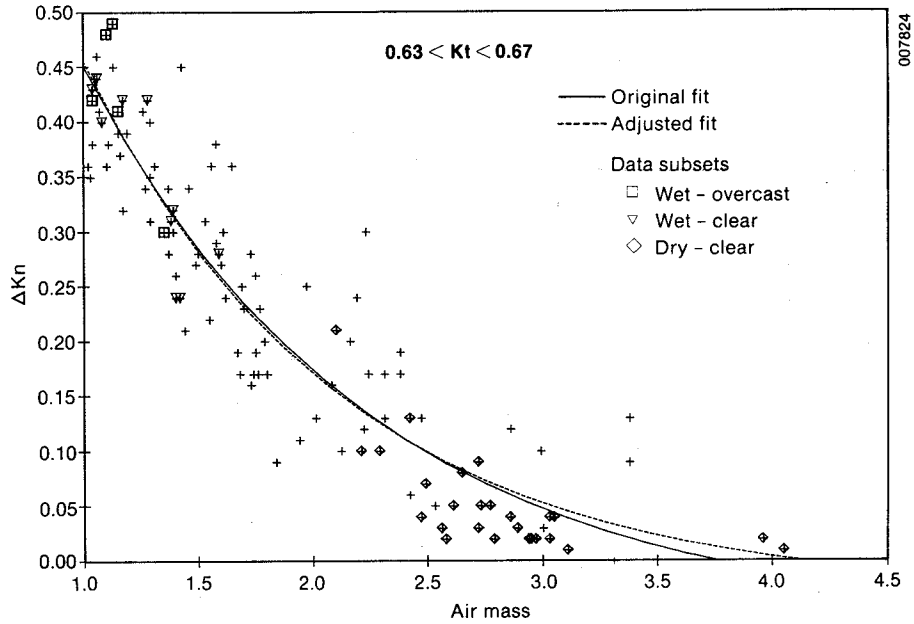


Figure 3-11(i). Scatter Plots of ΔKn vs. Air Mass and Exponential Fits for an Atlanta Data Subset ($0.63 < Kt < 0.67$) Used in Developing the Algorithms for the DISC Model

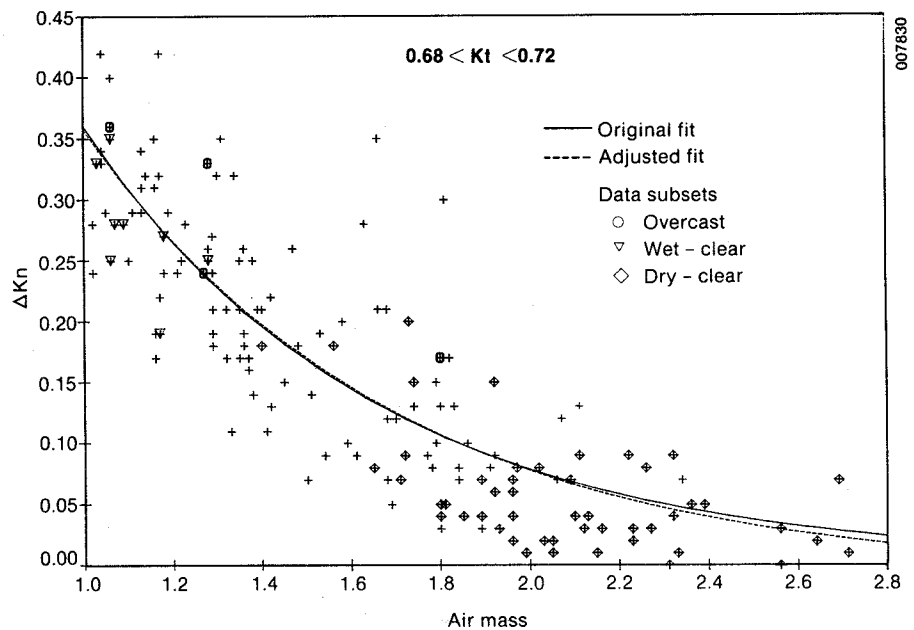


Figure 3-11(j). Scatter Plots of ΔKn vs. Air Mass and Exponential Fits for an Atlanta Data Subset ($0.68 < Kt < 0.72$) Used in Developing the Algorithms for the DISC Model

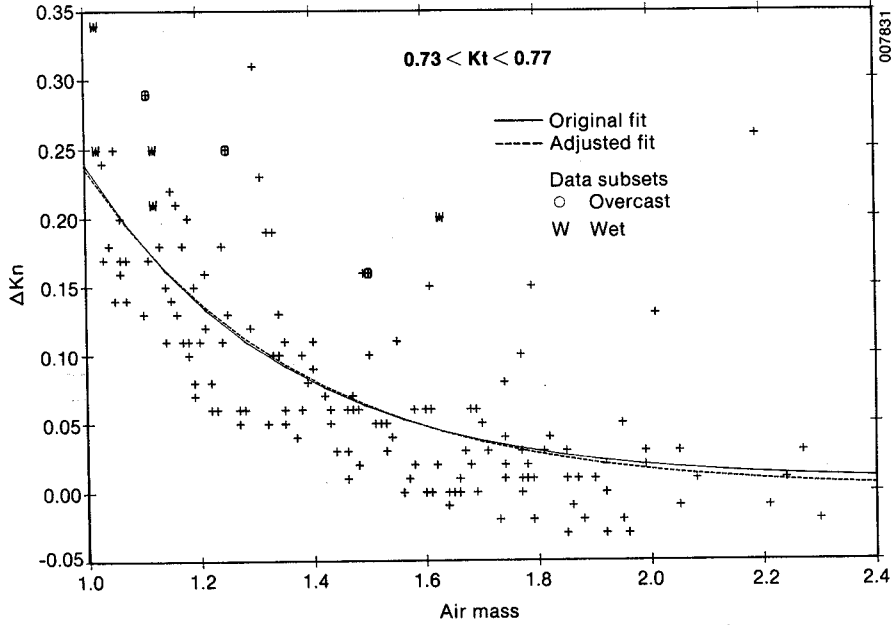


Figure 3-11(k). Scatter Plots of ΔKn vs. Air Mass and Exponential Fits for an Atlanta Data Subset ($0.73 < Kt < 0.77$) Used in Developing the Algorithms for the DISC Model

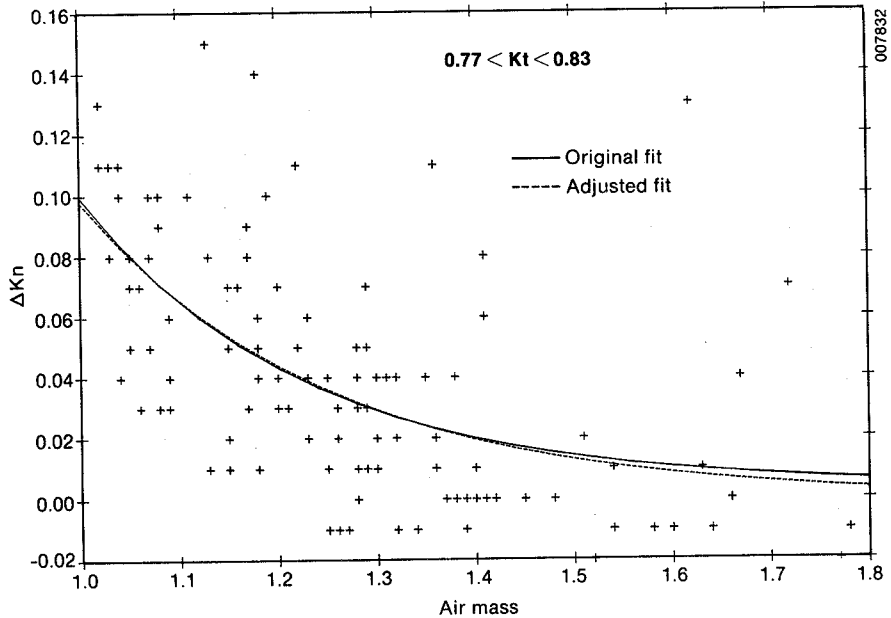


Figure 3-11(l). Scatter Plots of ΔKn vs. Air Mass and Exponential Fits for an Atlanta Data Subset ($0.77 < Kt < 0.83$) Used in Developing the Algorithms for the DISC Model

analysis. [The modified fit is shown as a dashed line on each of the curves in Figures 3-11(a)-(1).] The resulting set of functions relating air mass and ΔK_n is shown in Figure 3-12 and listed in Table 3-5. It is important to note that the Atlanta data set did not contain K_t values above 0.81. Therefore, the function for $K_t = 0.85$, shown in Figure 3-12, was established by plotting coefficients a , b , and c versus K_t and extrapolating these values to obtain coefficients for $K_t = 0.85$.

Figure 3-11(a) also contains the curve for Eq. (3-3), which represents K_n under clear-sky, dry atmospheric conditions. From this curve, it is apparent that if $K_t = 0.25$, the direct normal component of solar radiation is essentially equal to zero. In other words, when $\Delta K_n = K_{nc}$, the direct beam of radiation coming from the solar disk has been totally absorbed and/or scattered in the atmosphere, which is consistent with the results shown in Figures 2-1 and 3-4.

The special symbols in Figures 3-11(a)-(1) represent special cloud-cover and/or precipitable-water-vapor conditions and indicate the probability of future modifications to the model by incorporating terms for cloud cover and precipitable water vapor. For example, the C in Figure 3-11(c) identifies data points for which the sky was clear (i.e., there was 1/10 opaque cloud cover or less). The triangles on that same figure represent dry, overcast conditions when the opaque cloud cover was 9/10 or more and the precipitable water vapor was less than 1.5 cm. From these results, we can conclude that under clear atmospheric conditions, the ΔK_n should be less than that given by the function fit to all of the data points, and for dry, overcast conditions,

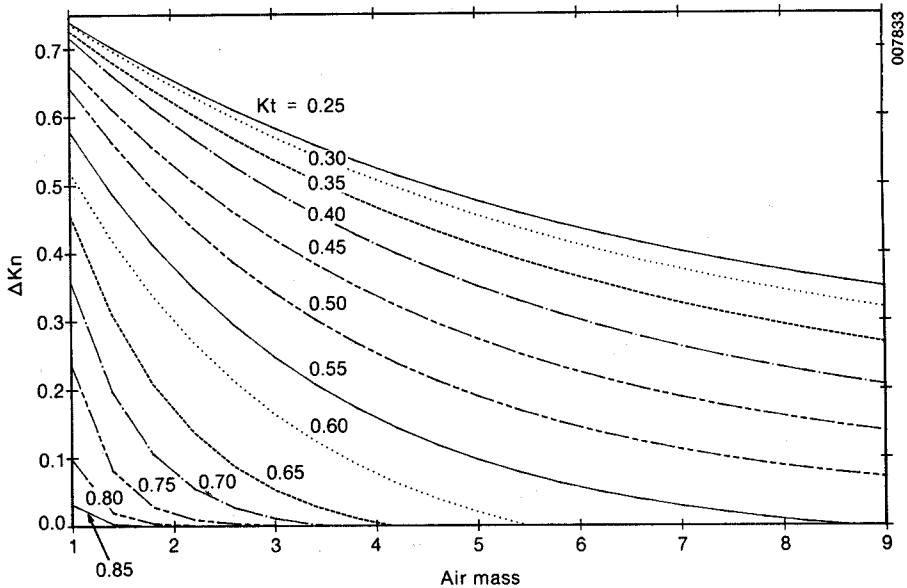


Figure 3-12. Thirteen Exponential Functions Relating ΔK_n and Air Mass

Table 3-5. Functions Relating ΔK_n and Air Mass (X)

Kt	Functions
0.25	$0.230 + 0.6108 * \text{EXP}(-0.1817*X)$
0.30	$0.190 + 0.6558 * \text{EXP}(-0.1813*X)$
0.35	$0.150 + 0.7026 * \text{EXP}(-0.1987*X)$
0.40	$0.110 + 0.7641 * \text{EXP}(-0.2313*X)$
0.45	$0.070 + 0.7971 * \text{EXP}(-0.2739*X)$
0.50	$0.030 + 0.8590 * \text{EXP}(-0.3380*X)$
0.55	$-0.030 + 0.9013 * \text{EXP}(-0.3930*X)$
0.60	$-0.080 + 0.9411 * \text{EXP}(-0.4500*X)$
0.65	$-0.030 + 1.1815 * \text{EXP}(-0.8890*X)$
0.70	$-0.010 + 1.5504 * \text{EXP}(-1.4399*X)$
0.75	$-0.001 + 3.2996 * \text{EXP}(-2.6362*X)$
0.80	$-0.001 + 5.1625 * \text{EXP}(-3.9549*X)$
0.85	$-0.001 + 8.0000 * \text{EXP}(-5.5000*X)$

the ΔK_n values should be larger. Similarly, for Figures 3-11(e) through 3-11(j), the data points marked with a diamond represent dry, clear conditions (i.e., the opaque cloud cover was 1/10 or less and the precipitable-water-vapor was less than 1.5 cm). The squares on these same figures represent wet overcast conditions where the opaque cloud cover is 9/10 or more and the precipitable-water-vapor is between 3.6 and 6.0 cm. Again, under dry, clear conditions, the ΔK_n values under the same airmass will be less than the curve indicates. Under wet, overcast conditions, there is no consistent change in ΔK_n as compared with the values represented by the curve. The equations for each of the curves shown in Figures 3-11 and 3-12 are given in Table 3-5.

Figure 3-13 is an enlargement of the higher Kt functions for Figure 3-12. Similarly, Figure 3-14 is an enlargement of the upper end of the lower Kt curve. These enlargements show greater detail and some of the remaining irregularities in these functional relationships.

3.2.3 Coefficient Functions

Initially, the values of the three coefficients a, b, and c were plotted versus Kt to establish a function for ΔK_n for Kt values of 0.85. As the plots of the coefficients were explained, however, it became apparent that they represented continuous functions with very little scatter or random variations. Therefore, we discarded the initial plan to use only the 13 functions given in Table 3-5 and chose to use polynomial functions to calculate coefficients for Eq. (3-4). This produced a continuous algorithm for calculating ΔK_n , K_n , and direct normal irradiance, representing as accurately as possible all values of Kt and air mass. Figures 3-15, 3-16, and 3-17 show the original coefficients and the curves generated by the polynomials used to calculate coefficients for the model. This represents the last step in the development of the current model, which is described in the next subsection.

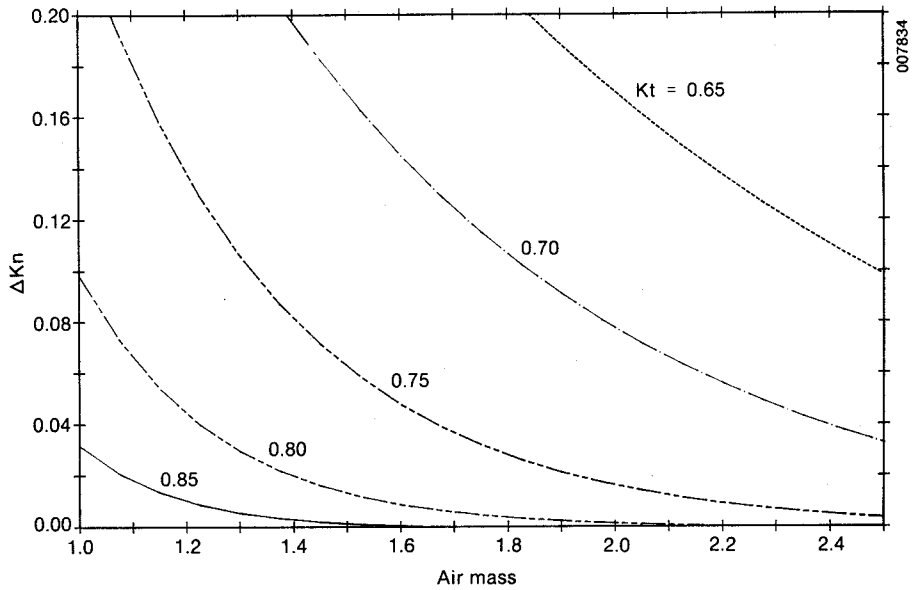


Figure 3-13. An Enlarged View of the High K_t Functions Relating ΔKn and Air Mass

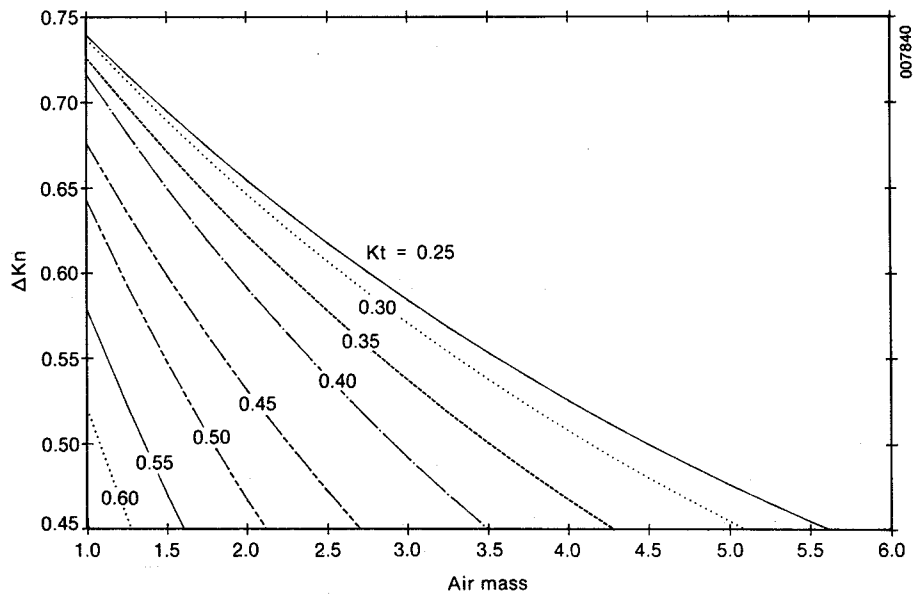
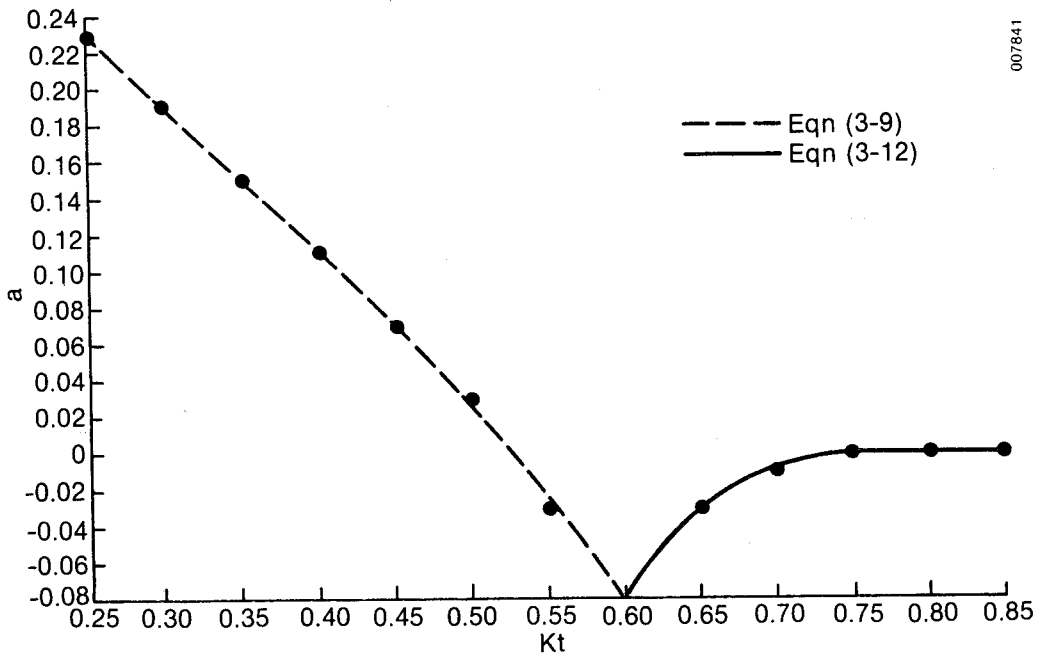
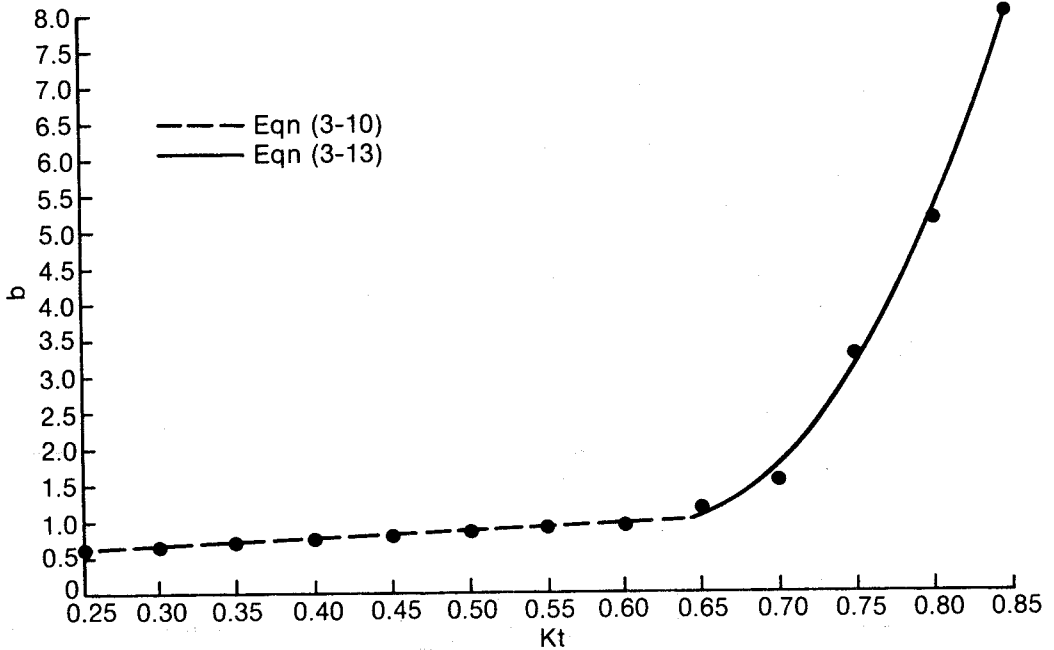


Figure 3-14. An Enlarged View of the Low K_t Functions Relating ΔKn and Air Mass



007841

Figure 3-15. Coefficient a (from the Exponential Functions Relating ΔKn and Air Mass) and the Two Polynomial Functions Fit to the a Data



007842

Figure 3-16. Coefficient b (from the Exponential Functions Relating ΔKn and Air Mass) and the Two Polynomial Functions Fit to the b Data

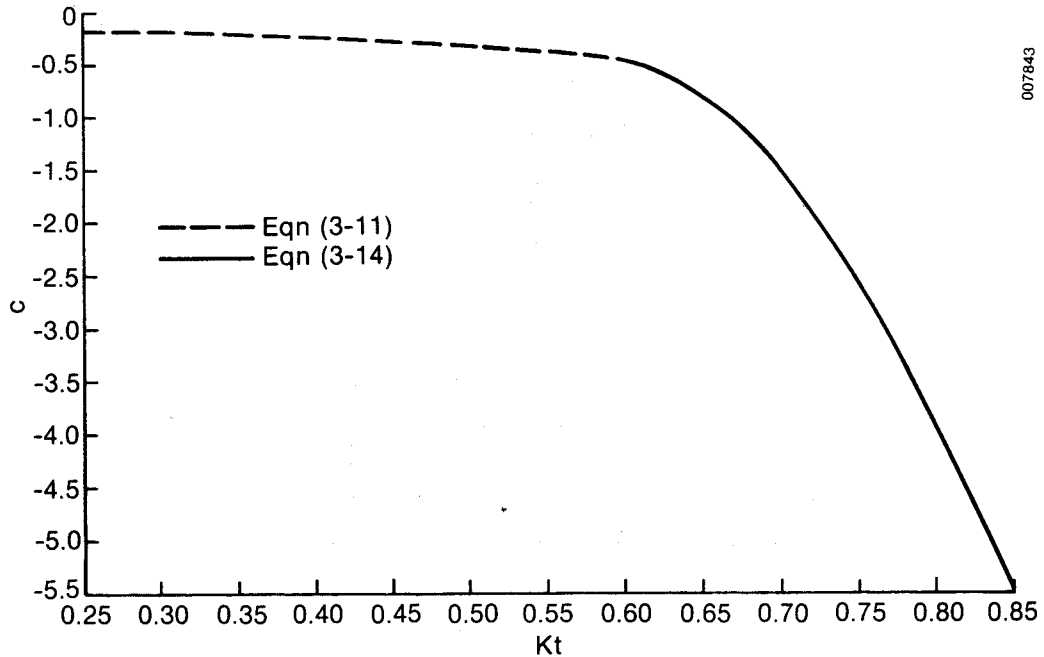


Figure 3-17. Coefficient c (from the Exponential Functions Relating ΔKn and Air Mass) and the Two Polynomial Functions Fit to the c Data

3.3 Description of the Model

The algorithms used to estimate direct normal irradiance from global horizontal data are shown in block diagram form in Figure 3-18. As indicated at the top of this figure, the input data to the model are global horizontal irradiance values for the time and place of interest. No other input data are required. These algorithms were activated through the development of a computer program called the Direct Insolation Simulation Code (DISC). DISC estimates the direct beam insolation arriving at the earth's surface from the solar disc. DISC is a very simple model requiring less than 100 lines of FORTRAN code that can be run on any computer (from a personal computer to the largest mainframe), as long as provision is made for using the required global horizontal insolation data. A complete description of the algorithms used in the DISC program follows.

To calculate Kt, the horizontal extraterrestrial radiation (I_{oh}) is calculated from the equations

$$r_e = 1.00011 + 0.034221 \cos \xi + 1.28 \times 10^{-3} \sin \xi + 7.19 \times 10^{-4} \cos 2\xi + 7.7 \times 10^{-5} \sin 2\xi , \quad (3-5)$$

and

$$I_{oh} = 1370 r_e \cos z , \quad (3-6)$$

007844

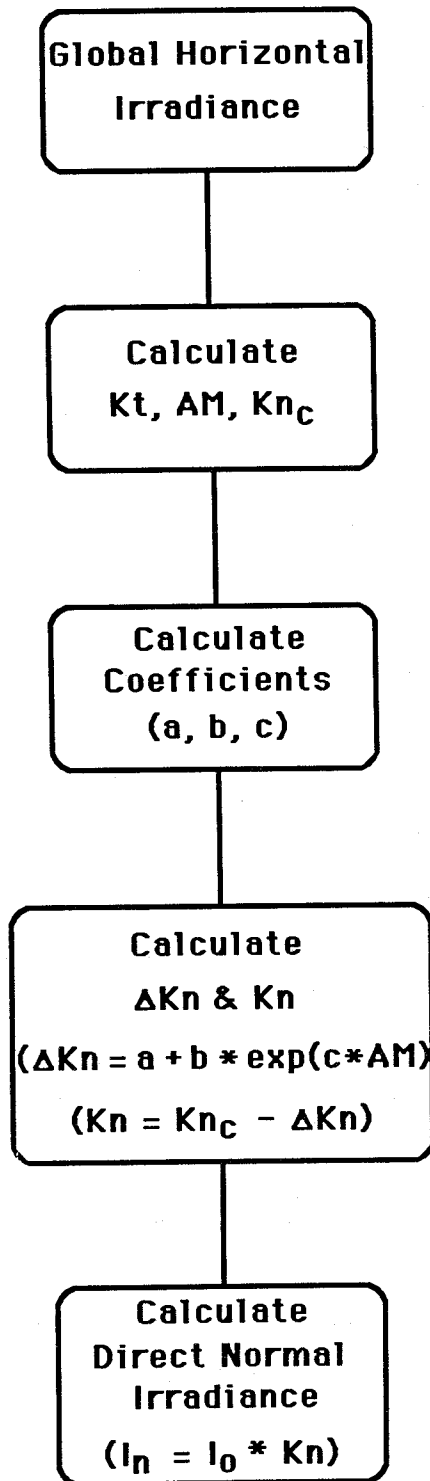


Figure 3-18. Block Diagram of the DISC Model for Estimating Direct Normal Insolation from Observed Global Horizontal Insolation Data

where

ξ = the eccentric anomaly of the earth in its orbit around the sun

z = the sun's zenith angle

r_e = the reciprocal of the square of the earth radius vector (Spencer 1971)

and

1370 = the solar constant (W/m^2) (WMO 1981; Hickey et al. 1986).

K_t is then calculated according to

$$K_t = I_t / I_{oh} , \tag{3-7}$$

where

I_t = the measured total global horizontal irradiance at the surface of the earth.

Air mass is then calculated using an expression from Kasten (1966),

$$(AM) = [\cos z + 0.15(93.885 - z)^{-1.253}]^{-1} , \tag{3-8}$$

and the direct beam atmospheric transmittance under clear-sky conditions (Kn_c) is calculated using Eq. (3-3).

Next, the coefficients used in calculating ΔKn are determined using equations grouped for two K_t ranges.

If $K_t \leq 0.60$,

$$a = 0.512 - 1.56 K_t + 2.286 K_t^2 - 2.222 K_t^3 \tag{3-9}$$

$$b = 0.370 + 0.962 K_t \tag{3-10}$$

$$c = -0.280 + 0.932 K_t - 2.048 K_t^2 . \tag{3-11}$$

If $K_t > 0.60$,

$$a = -5.743 + 21.77 K_t - 27.49 K_t^2 + 11.56 K_t^3 \tag{3-12}$$

$$b = 41.40 - 118.5 K_t + 66.05 K_t^2 + 31.90 K_t^3 \tag{3-13}$$

$$c = -47.01 + 184.2 K_t - 222.0 K_t^2 + 73.81 K_t^3 . \tag{3-14}$$

Finally, employing the coefficients calculated above, we calculate ΔKn , Kn , and I_n using the equations

$$\Delta Kn = a + b \exp[C * (AM)] \tag{3-15}$$

$$Kn = Kn_c - \Delta Kn \tag{3-16}$$

and

$$I_n = I_o * Kn . \tag{3-17}$$

4.0 VERIFICATION AND VALIDATION OF THE MODEL

Model verification tests the accuracy of the FORTRAN code developed for the model, coefficients for the equations, and all other procedures and calculations conducted during the operation of the model. In this study, the verification of the model was accomplished using the same Atlanta data sets employed in developing the model.

The validation of the DISC model was accomplished using data from other stations at widely varying latitudes with significantly different climates. For comparison, we evaluated the ETMY model, used to generate all of the direct normal data in the Ersatz TMY data base, against the same data sets. To avoid the extreme conditions encountered at low solar elevations, data for zenith angles greater than 85.5 deg were excluded from these tests. The DISC algorithms for computing zenith angles, air mass, the earth's radius vector, and extraterrestrial radiation were used with the ETMY direct normal insolation algorithm. This ensured that the comparisons of the two models would evaluate only the differences in the methods of calculating insolation.

The ADIPA model was not used for comparison with the DISC model since the statistical term $y(Kt, \chi)$ employed in that model would have introduced a random difference similar to Gaussian noise. This action would affect RMS errors in a manner unrelated to the model's ability to simulate the transfer of direct beam solar radiation through the atmosphere. When cloud-cover and water-vapor terms have been added to the model, we will compare the statistical distributions of hourly values from SOLMET, Ersatz, measured, and DISC data sets.

4.1 Methods of Analysis

To verify the correctness of the code written for the model, global horizontal values from the Atlanta data set were used as input. Calculated direct normal insolation estimates were then compared with measured insolation estimates. The difference and percent difference between hourly values were calculated from

$$D = Y - X , \quad (4-1)$$

and

$$\%D = [(Y - X)/X] * 100 , \quad (4-2)$$

where

Y = a model calculated value

and

X = a measured value of direct normal insolation.

In addition to differences and percent differences for each hourly value, mean differences, percent mean differences, RMS differences, and percent RMS differences were calculated for each month. Because of the long-standing convention of referring to these differences as mean bias errors (MBE) and root mean square errors (RMSE), we will use this terminology in the following discussions. However, both the measured data and the modeled data may be in error

relative to the true direct normal insolation at the location, hour, and day to which the modeled and measured values apply. Therefore, although we will refer to mean bias errors and RMS errors, these are really mean differences and RMS differences between measured and calculated data.

RMSE is defined as

$$\text{RMSE} = \left[n^{-1} \sum_{i=1}^n (Y_i - X_i)^2 \right]^{0.5}, \quad (4-3)$$

where

n = sample size,

Y_i = a model generated value for time interval i ,

and

X_i = a corresponding measured value.

This error provides a measure of the random variability in the difference between measured and modeled data. The percent RMSE is most often plotted or tabulated and it is calculated according to

$$\% \text{RMSE} = 100(\text{RMSE}/\bar{X}), \quad (4-4)$$

where \bar{X} is the measured mean direct normal insolation for the month.

MBE is calculated by

$$\text{MBE} = n^{-1} \sum_{i=1}^n (Y_i - X_i), \quad (4-5)$$

which provides a measure of the mean offset or bias between the modeled and measured values. The percent MBE is calculated according to

$$\% \text{MBE} = 100(\text{MBE}/\bar{X}). \quad (4-6)$$

4.2 Verification Results

In the initial verification tests, we detected some problems in the original computer code. These were corrected and the tests were repeated. The results shown here are from the final round of tests, after all corrections were made to the code. The %RMSE and %MBE for the DISC and ETMY models for 1981 Atlanta data are given in Figures 4-1 and 4-2. Since RMS errors provide a measure of the ability of the model to respond to hourly variations of solar elevation and atmospheric conditions, the reduction in %RMSE shown in Figure 4-1 is more significant than the reduced %MBE shown in Figure 4-2. The combined reductions in %RMSE and %MBE as shown in Figures 4-1 and 4-2 are most encouraging.

The mean bias errors were usually negative during fall and winter months and positive during spring and summer months. When compared with concurrent

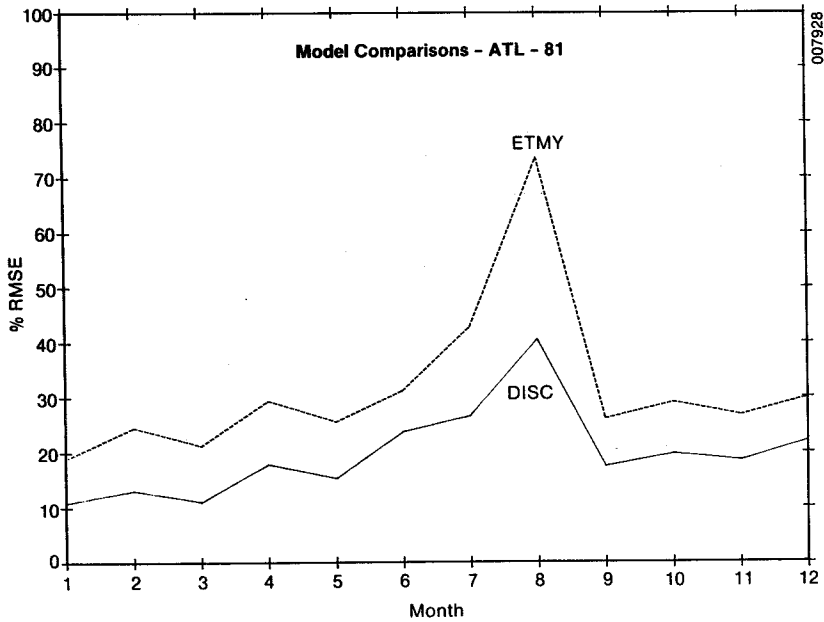


Figure 4-1. Percent RMS Differences between Estimated (DISC and ETMY Models) and Observed Direct Normal Insolation Values for 1981 Data from Atlanta, Ga.

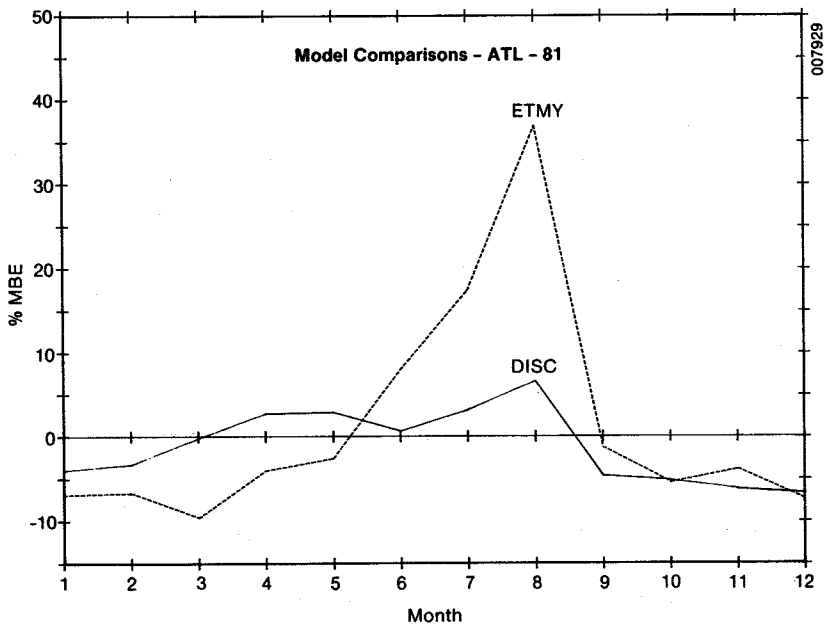
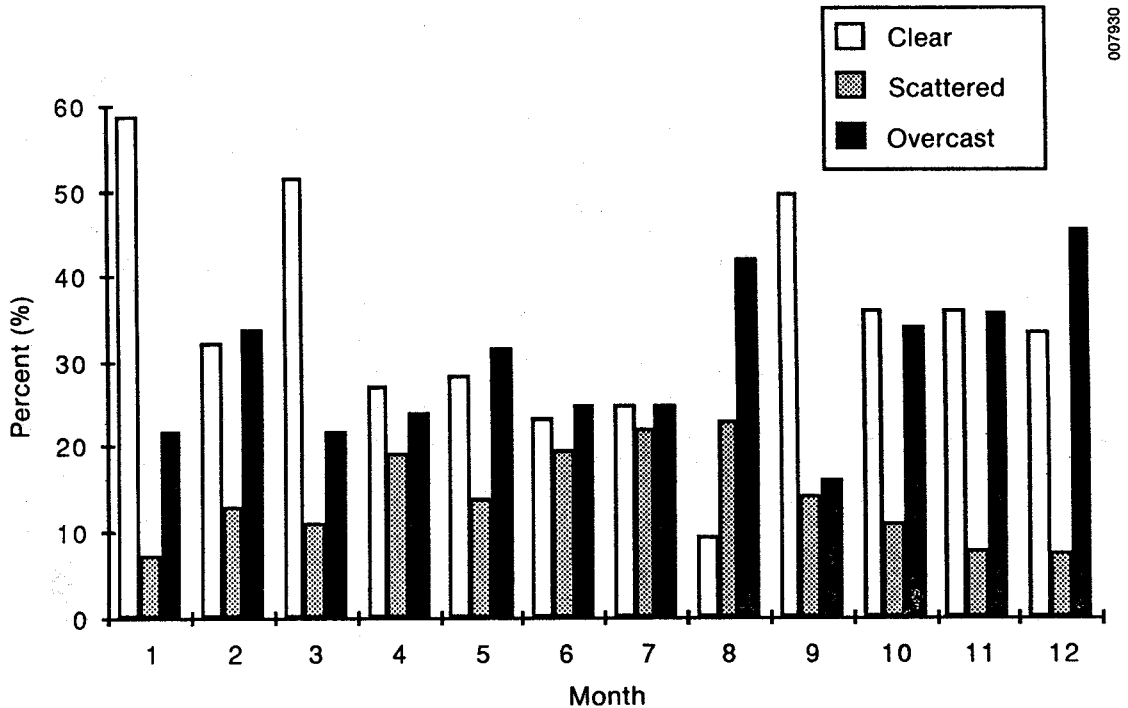


Figure 4-2. Percent Mean Bias Differences between Estimated (DISC and ETMY Models) and Observed Direct Normal Insolation Values for 1981 Data from Atlanta, Ga.

cloud-cover conditions for Atlanta, shown in Figure 4-3, it appears that the increased incidence of scattered clouds during the spring and summer months produced a positive MBE. Scattered and overcast conditions dominated the sky during August 1981 at Atlanta, producing the largest positive MBE for both models.

During the fall and winter months of 1981, the sky at Atlanta alternated between clear and overcast conditions. Under overcast conditions, the direct beam is essentially nonexistent, so the negative MBE observed during these months occurred under clear skies. These results are entirely consistent with the tendency of data points for dry, clear conditions to fall below the curves of Figures 3-11(a)-(1) and for data points for cloudy, wet conditions to fall above the same curves. Furthermore, this indicates that the model might be improved by adding cloud-cover and precipitable-water functions.

The plot of hourly errors (see Figures 4-4 and 4-5) for June 14, 1981, a clear day, and June 28, 1981, a partly cloudy day, show a significant improvement in the diurnal performance of the DISC model when compared with the ETMY model. The diurnal pattern still apparent in these plots indicates that the compensation for air mass variations is still not adequate. Furthermore, these results confirm the need for a cloud-cover modifier to effect additional improvements in the performance of the model. Such improvements will be pursued in future work.



007830

Figure 4-3. Percentage of All Hours for Which Clear (0 to 0.1), Scattered (0.4 to 0.6), and Overcast (0.9 to 1.0) Cloud-Cover Conditions were Observed at Atlanta in 1981

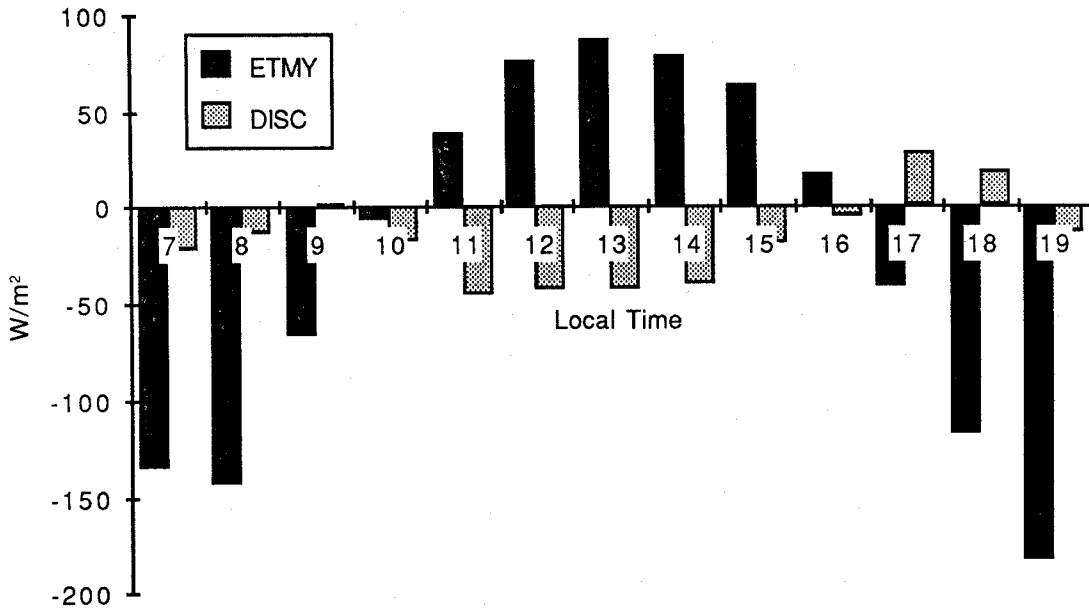


Figure 4-4. Estimated (ETMY and DISC Models) Minus Observed Differences in Hourly Means of Direct Normal Insolation from Atlanta, Ga., on June 14, 1981 (Clear-sky conditions)

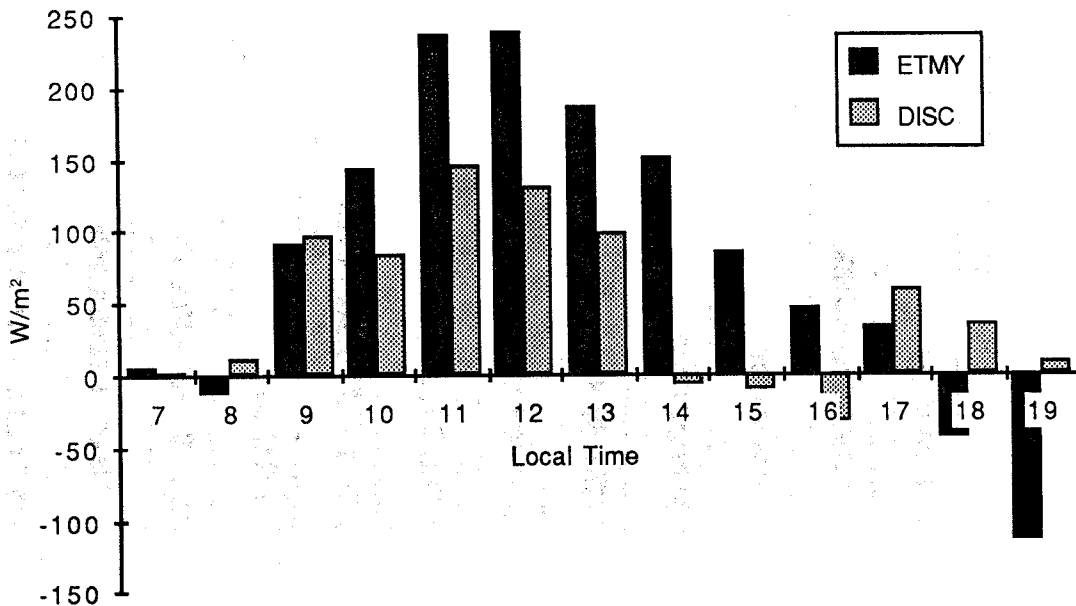


Figure 4-5. Estimated (ETMY and DISC Models) Minus Observed Differences in Hourly Means of Direct Normal Insolation from Atlanta, Ga., on June 28, 1981 (Scattered-cloud conditions)

4.3 Validation Results

Three stations, representing significantly different climate conditions, were selected to validate this model. A list of these three stations and pertinent information about each one follow.

- Station: Brownsville, Tex.
Latitude: North 25° 54'
Longitude: West 97° 26'
Elevation: 6 m
Climate type: Subtropical, subhumid

- Station: Albuquerque, N.M.
Latitude: North 35° 3'
Longitude: West 106° 37'
Elevation: 1619 m
Climate type: Temperate, arid

- Station: Bismarck, N.D.
Latitude: North 46° 46'
Longitude: West 100° 45'
Elevation: 502 m
Climate type: Cold, temperate, semiarid

Each station was part of the new NOAA Solar Radiation Network and had a good record of both global horizontal and direct normal insolation data. Data from one year were selected from each station for the validation tests.

4.3.1 Results for Brownsville, Texas

The %MBE and %RMSE for both the ETMY and DISC models are shown in Figures 4-6 and 4-7. In general, the %MBE for the two models are similar; the DISC model showed better results during the first half of the year and the ETMY model produced better results during the second half. The DISC model, however, exhibited lower RMS errors during the entire year, except during May.

Figure 4-8 is a plot of cloud-cover conditions for Brownsville during 1980 that shows a dominance of overcast conditions during the winter months. This gives way to clear or scattered cloud conditions during the summer. The sharp transition from overcast to clear conditions between May and June is reflected in the %MBE change shown in Figure 4-6. The %MBE for December, however, does not reflect the return to wintertime conditions. Obviously, factors other than opaque cloud cover affect the performance of the models, such as type of clouds, total cloud cover, precipitable water vapor in the atmosphere, and turbidity.

Hourly errors for January 23, 1980, are shown in Figure 4-9. On this date, the opaque cloud cover varied from 0.7 to 1.0 over the entire day. Under these conditions, which are typical for Brownsville winters, both models exhibited a great deal of variability in their performance. Yet overall, the DISC model gave better results for this day.

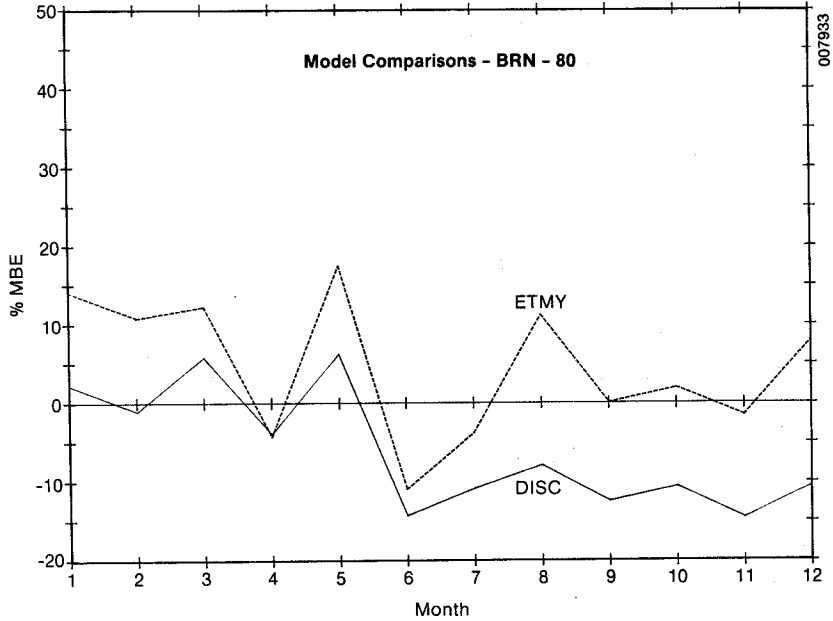


Figure 4-6. Percent Mean Bias Differences between Estimated (DISC and ETMY Models) and Observed Direct Normal Insolation Values for 1980 Data from Brownsville, Tex.

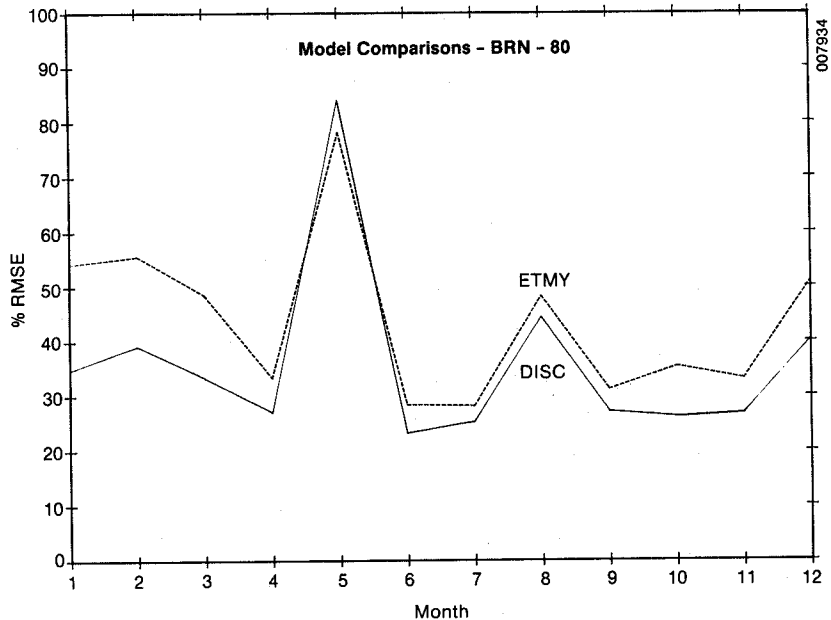


Figure 4-7. Percent RMS Differences between Estimated (DISC and ETMY Models) and Observed Direct Normal Insolation Values for 1980 Data from Brownsville, Tex.

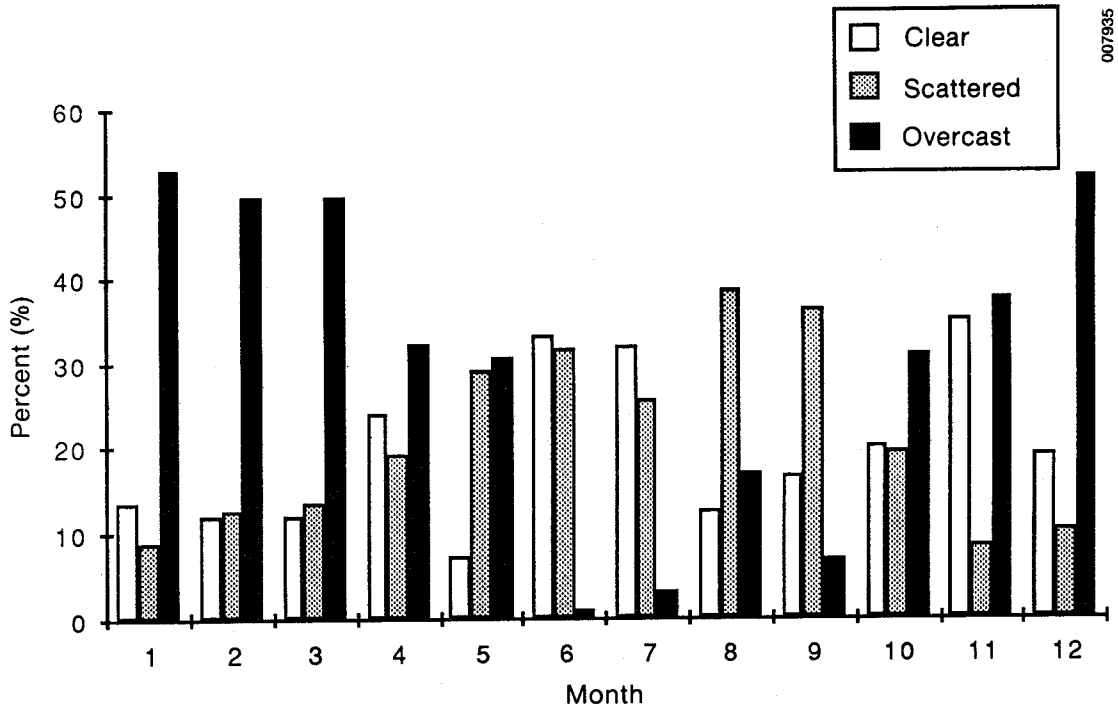


Figure 4-8. Percentage of All Hours for which Clear (0 to 0.1), Scattered (0.4 to 0.6), and Overcast (0.9 to 1.0) Cloud-Cover Conditions Were Observed at Brownsville in 1980

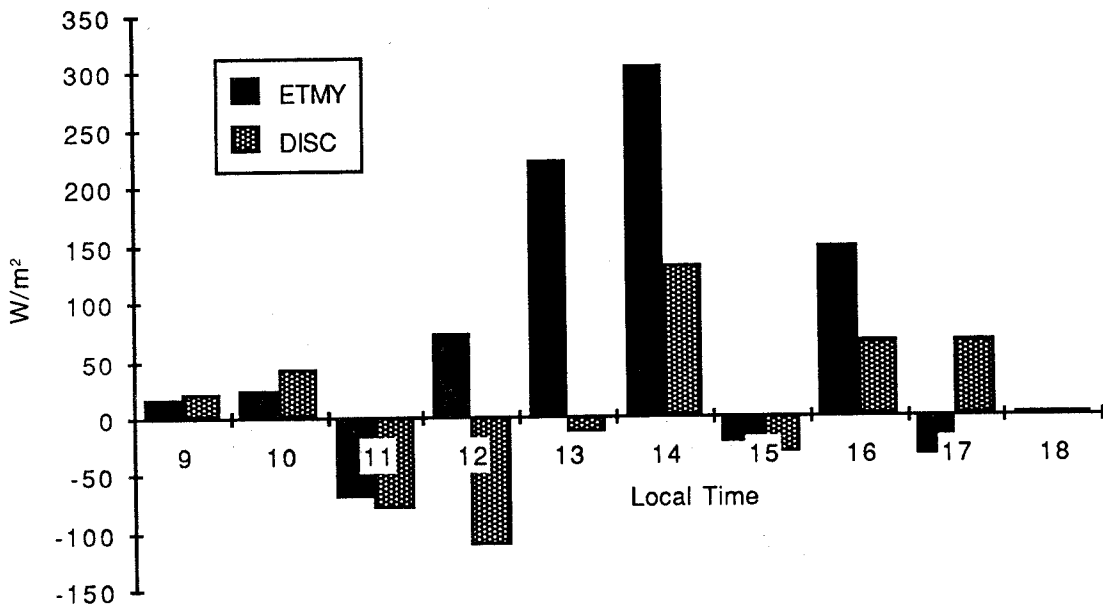


Figure 4-9. Estimated (ETMY and DISC Models) Minus Observed Differences in Hourly Means of Direct Normal Insolation for Brownsville, Tex., on January 23, 1980 (0.7 to 1.0 cloud cover)

4.3.2 Results for Albuquerque, New Mexico

Both the DISC and the ETMY models produced very acceptable results for Albuquerque during 1979, as shown in Figure 4-10. The DISC model generally estimated values higher than the measurements, whereas the ETMY model estimated values lower than the measurements. Because of the generally clear atmospheric conditions that prevailed during the entire year (see Figure 4-11), we would expect that both models would estimate values lower than measurements. The reason for this deviation is not understood at this time.

The DISC model shows consistently improved RMS errors for all months (see Figure 4-12), probably as a result of smaller diurnal variations for October 6, 1979, and October 9, 1979 (Figures 4-13 and 4-14, respectively). October 6 was a very clear day, whereas on October 9, the opaque cloud cover varied from 0.3 at 7:00 a.m. to 0.9 at 5:00 p.m. The almost constant error for the DISC model from 8:00 a.m. to 4:00 p.m. on October 6 represents a percentage error of -7% to -8% and indicates that the air-mass correction for the DISC model is working very well.

4.3.3 Results for Bismarck, North Dakota

The differences between the model's estimated and the measured direct normal insolation values for Bismarck, N.D., during 1980 represent some of the more interesting validation results. As shown in Figure 4-15, both the DISC and the ETMY models produced very high estimates for the winter months. The RMS errors were also very high for these months, as indicated in Figure 4-16. The cloud-cover data for Bismarck in 1980, as plotted in Figure 4-17, show a mixture of overcast, scattered, and clear conditions during most months of the year. After examining the errors for individual hours of individual days, we found many days with high opaque cloud cover ranging from 0.7 to 1.0, for which the measured direct normal insolation was zero or close to zero. For these same hours, the model's estimated direct normal insolation was quite high (e.g., on February 28, the value recorded at 11:00 a.m. was 5 W/m^2 , whereas the DISC model estimated 475 W/m^2 and the ETMY estimated 476 W/m^2). The opaque cloud cover observed at this hour was 0.8. Figure 4-18 shows the hourly errors for February 27, 1980, during which the opaque cloud cover was a uniform 0.9, except for the first 2 hours of the day when the cloud cover was 1.0. With the exception of 4 p.m., the measured direct normal insolation never exceeded 5 W/m^2 . Between 3 p.m. and 4 p.m., the measured direct normal insolation was 299 W/m^2 , whereas the estimated values were 801 W/m^2 for the DISC model and 724 W/m^2 for the ETMY model. Apparently a break in the clouds allowed the solar beam to irradiate the radiometers during this hour.

For the infrequent clear atmospheric conditions during February, both models underestimated the actual measured direct normal irradiance, as shown in Figure 4-19. One possible explanation for these contrasting results hypothesizes a very high surface albedo (e.g., snow cover) producing abnormally high global horizontal insolation values under partly cloudy and even overcast conditions, caused by multiple reflections between the surface of the earth and the cloud layer. These multiple reflections would not, however, result in high direct normal insolation, since the direct beam radiation from the solar disc would be almost totally scattered and/or absorbed by the clouds. Since both of these models estimate direct normal insolation based on global

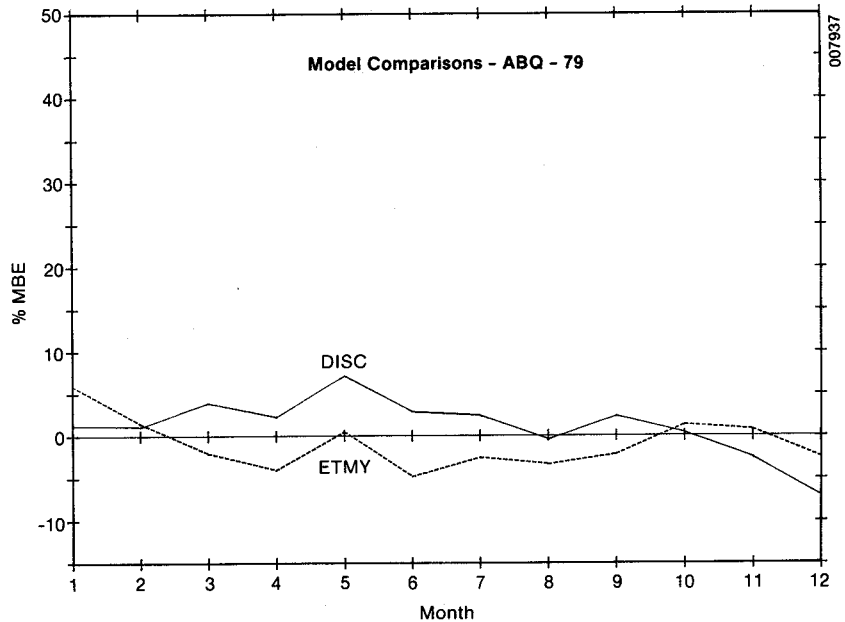


Figure 4-10. Percent Mean Bias Differences between Estimated (DISC and ETMY Models) and Observed Direct Normal Insolation Values for 1979 Data for Albuquerque, N.M.

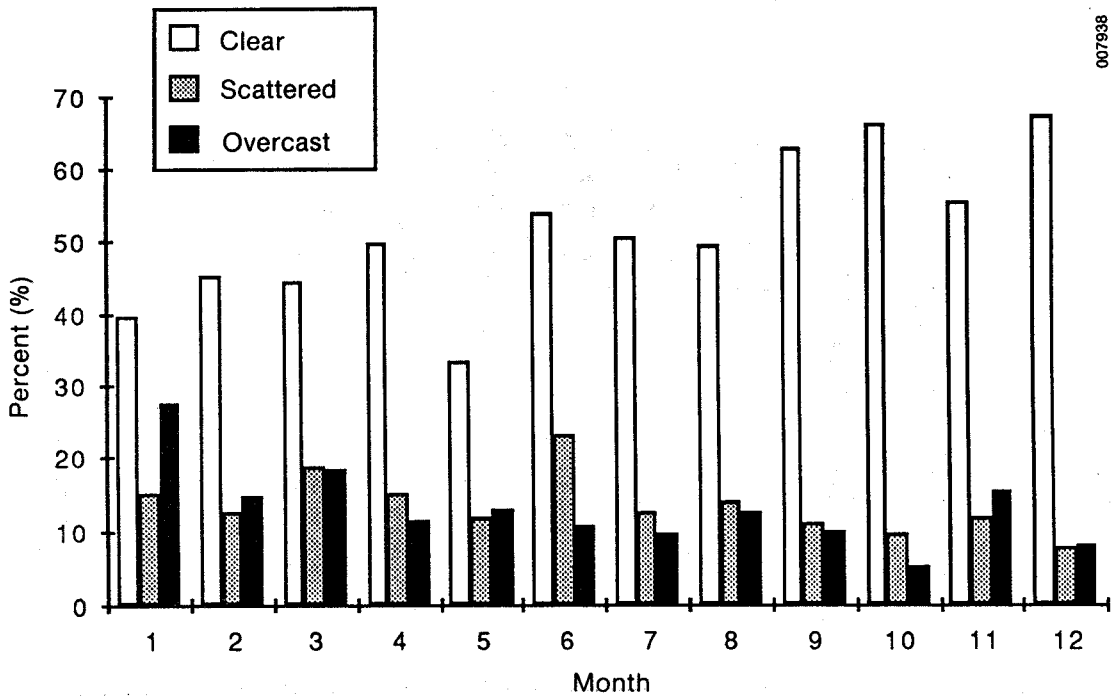


Figure 4-11. Percentage of All Hours for Which Clear (0 to 0.1), Scattered (0.4 to 0.6), and Overcast (0.9 to 1.0) Cloud-Cover Conditions Were Observed at Albuquerque in 1979

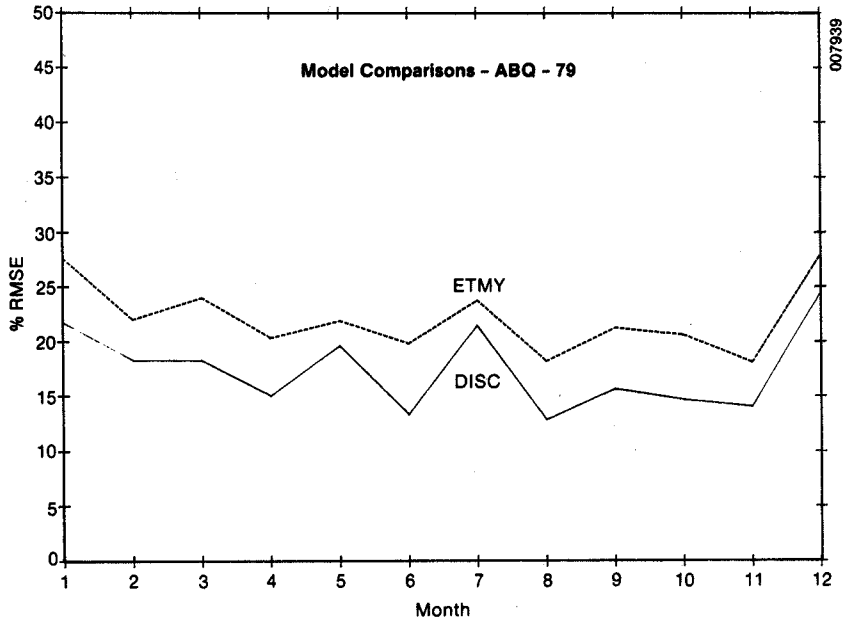


Figure 4-12. Percent RMS Differences between Estimated (DISC and ETMY Models) and Observed Direct Normal Insolation Values for 1979 Data from Albuquerque, N.M.

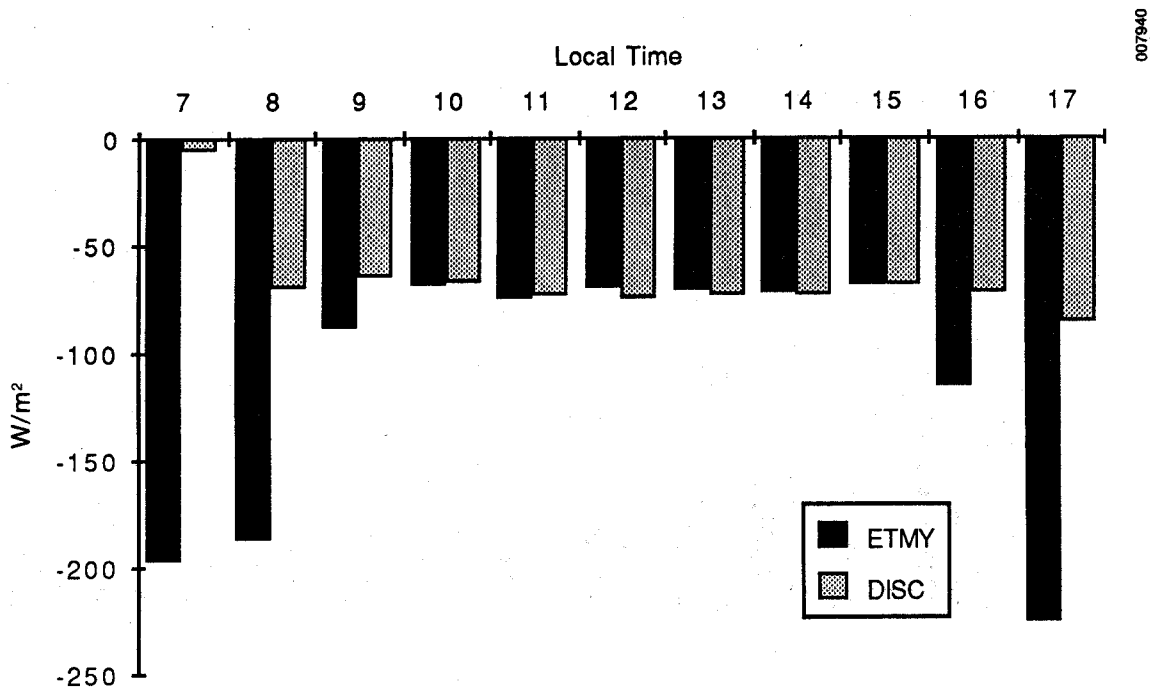


Figure 4-13. Estimated (ETMY and DISC Models) Minus Observed Differences in Hourly Means of Direct Normal Insolation for Albuquerque, N.M., on October 6, 1979 (Clear-sky conditions)

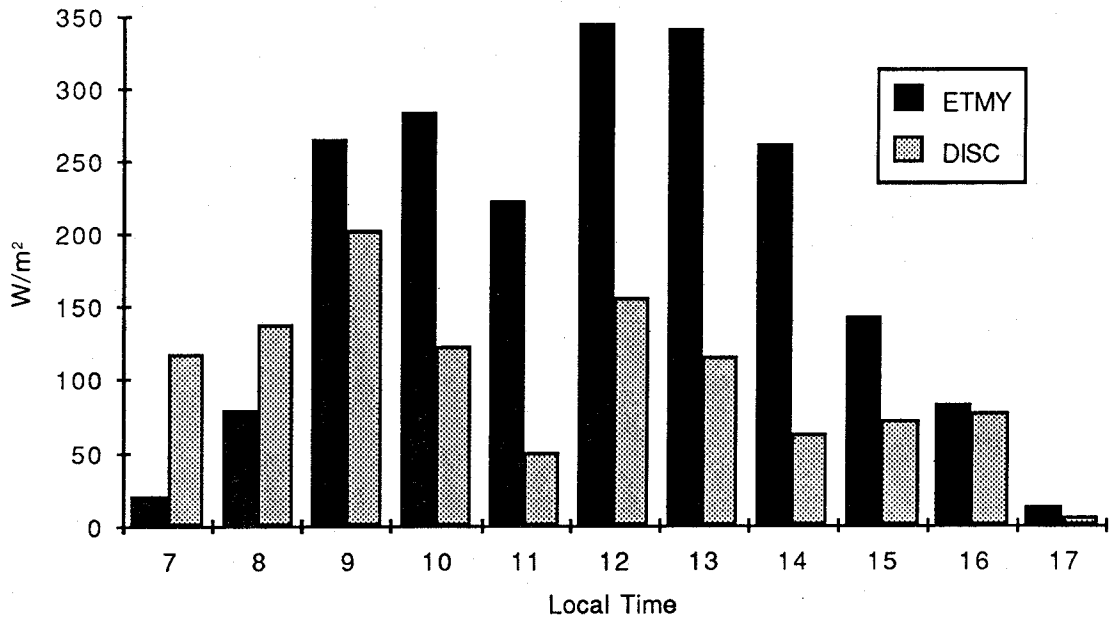


Figure 4-14. Estimated (ETMY and DISC Models) Minus Observed Differences in Hourly Means of Direct Normal Insolation for Albuquerque, N.M., on October 9, 1979 (0.3 to 0.9 cloud cover)

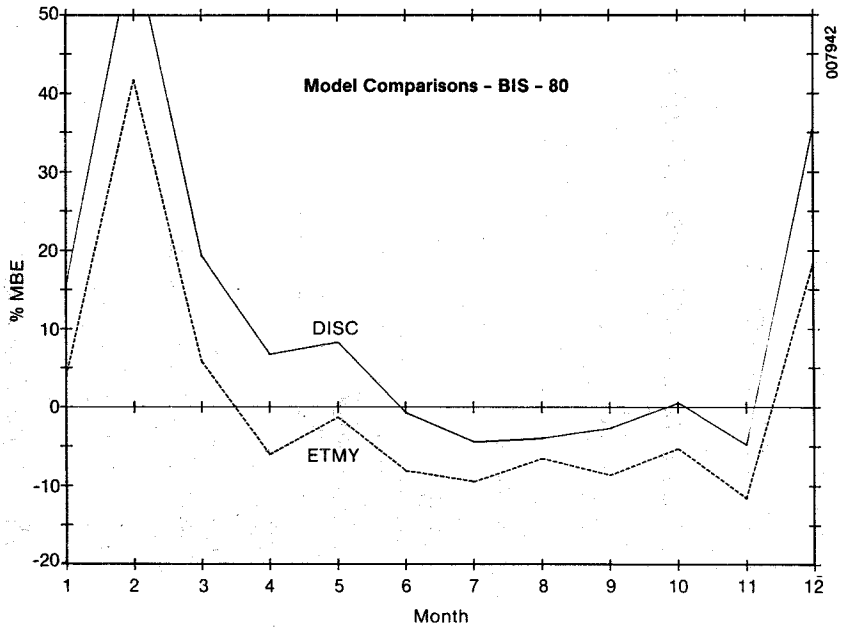


Figure 4-15. Percent Mean Bias Differences between Estimated (DISC and ETMY Models) and Observed Direct Normal Insolation Values for 1980 Data from Bismarck, N.D.

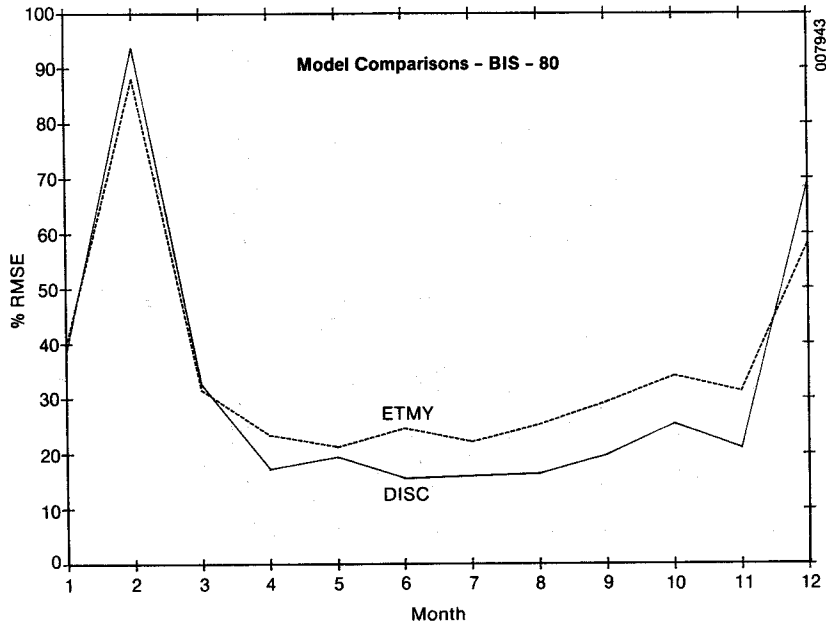


Figure 4-16. Percent RMS Differences between Estimated (DISC and ETMY Models) and Observed Direct Normal Insolation Values for 1980 Data from Bismarck, N.D.

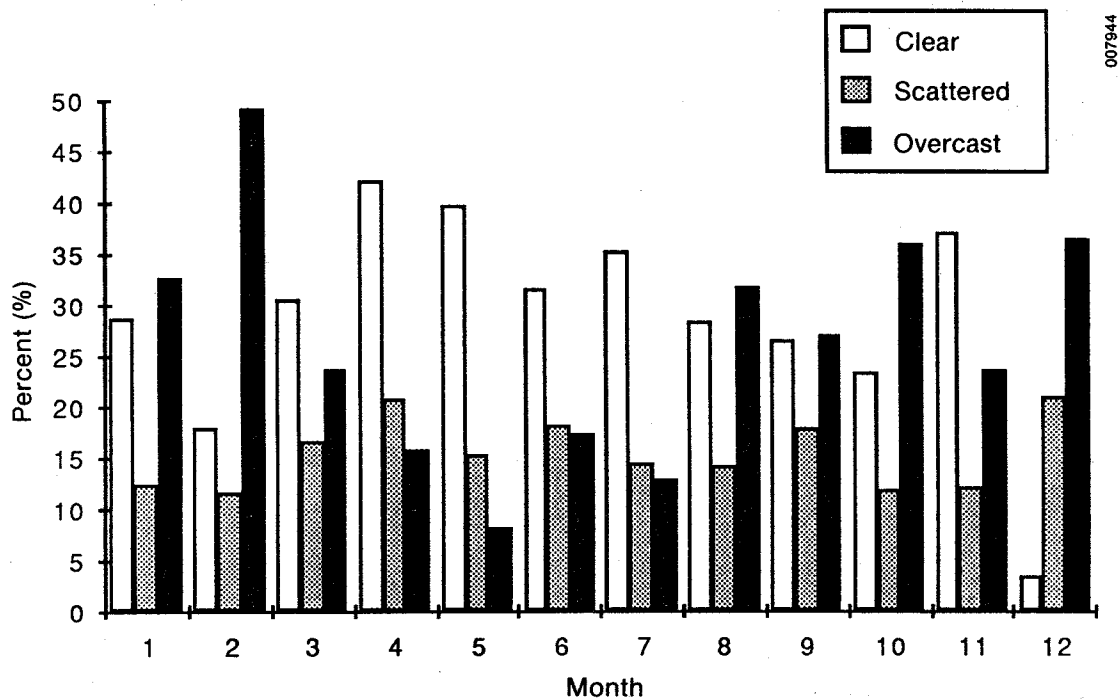


Figure 4-17. Percentage of All Hours for Which Clear (0 to 0.1), Scattered (0.4 to 0.6), and Overcast (0.9 to 1.0) Cloud-Cover Conditions Were Observed at Bismarck in 1980

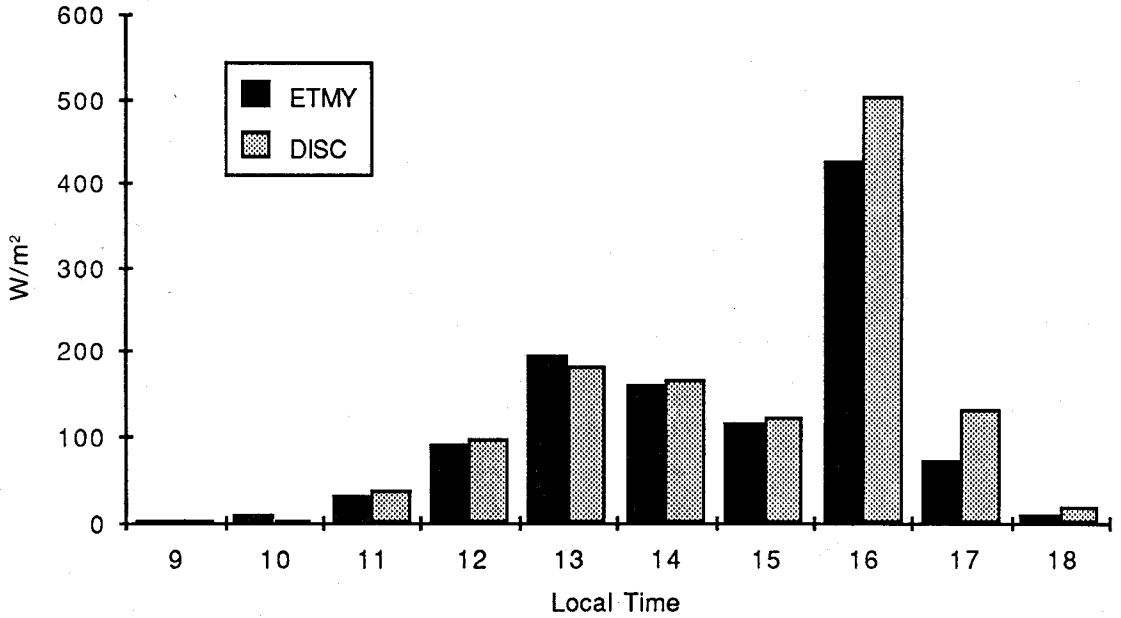


Figure 4-18. Estimated (ETMY and DISC Models) Minus Observed Differences in Hourly Means of Direct Normal Insolation from Bismarck, N.D., on February 27, 1980 (0.9 to 1.0 cloud cover, probable snow cover on the ground)

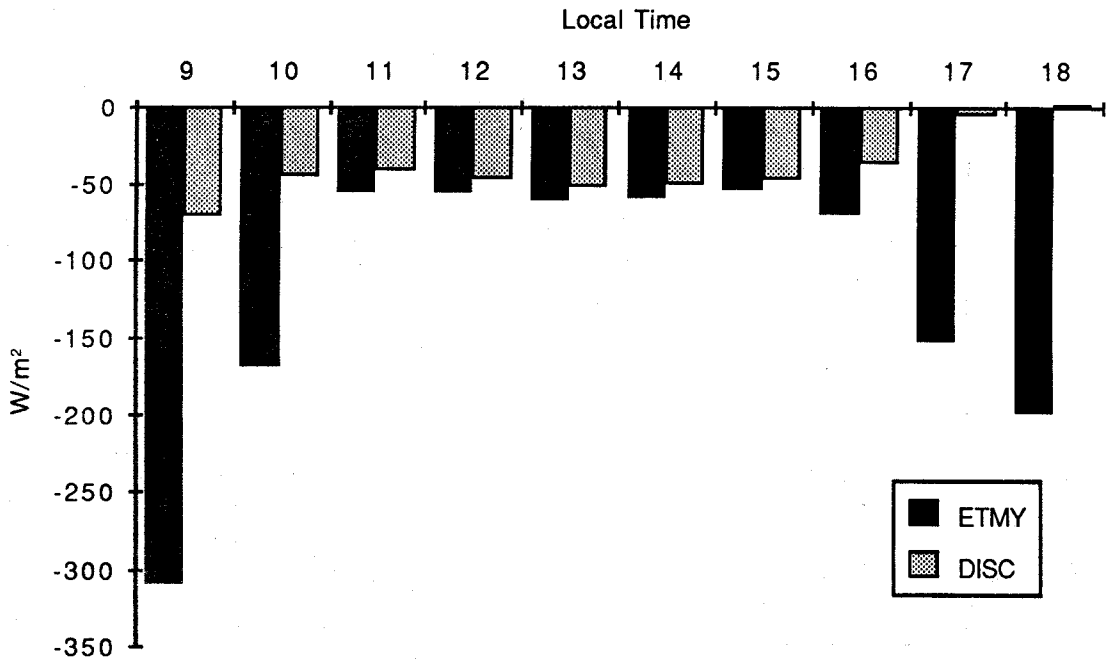


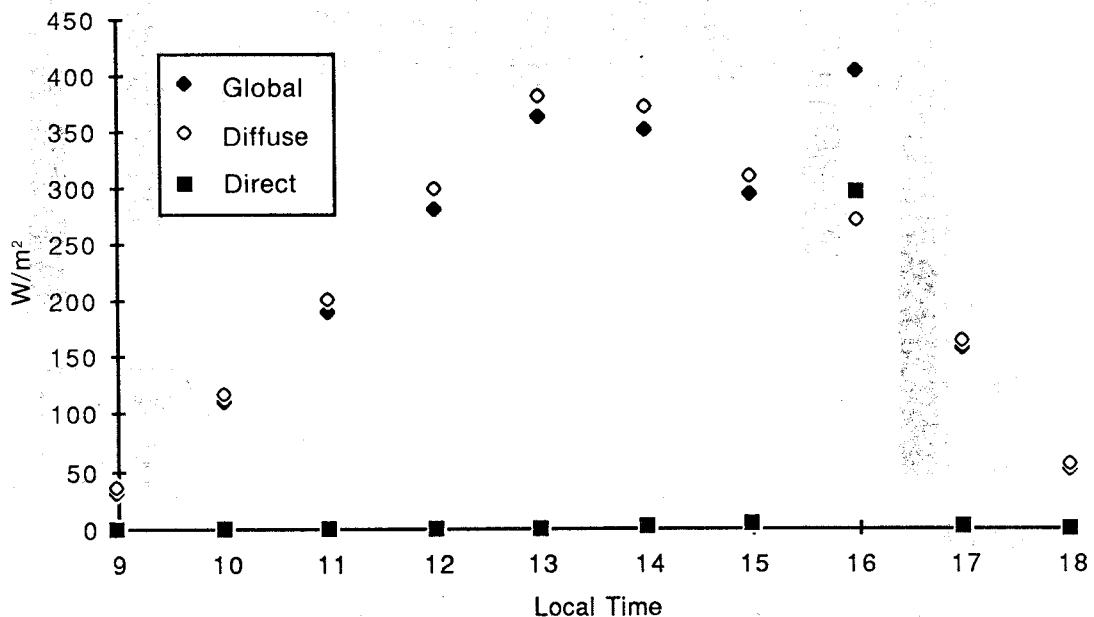
Figure 4-19. Estimated (ETMY and DISC Models) Minus Observed Differences in Hourly Means of Direct Normal Insolation from Bismarck, N.D., on February 26, 1980 (Clear-sky conditions, probable snow cover on the ground)

horizontal values, the abnormally high global horizontal measurements result in high estimates of the direct normal insolation.

Snow cover on the ground at Bismarck, N.D., is very common during the winter; weather records for 1980 reported that the snowfall during January, February, and March was 12.6 inches, 5.6 inches, and 5.7 inches, respectively. Snow fell on more than 5 days during January, more than 2 days during February, and more than 1 day in March. Given monthly mean temperatures of 11.2°, 15.4°, and 24.8°F for the respective months, the results shown in Figures 4-15 and 4-16 are readily understandable. We should also note that 4.7 inches of snow fell in December, with no more than 1.1 inches on any given day. This is also consistent with the results of the model comparisons.

One might also hypothesize that poor tracker performance, under the severe winter conditions at Bismarck, could have caused these results. Fortunately, Bismarck is one of the few NOAA stations that measured diffuse horizontal irradiance as well as the global horizontal and direct normal components. Therefore, we were able to resolve this issue by examining all three components. As shown in Figure 4-20, diffuse irradiance is contributing all of the global horizontal irradiance on February 27, 1980, except from 3 p.m. to 4 p.m. Diffuse values that are slightly greater than global values are most likely the result of an error in the shadow-band correction.

Given all of the evidence, we conclude that a snow-covered, high-albedo surface caused the models to perform poorly. We intend to investigate this further and will attempt to develop an albedo correction term for the DISC model.



007947

Figure 4-20. Global, Diffuse, and Direct Irradiance at Bismarck, N.D., on February 27, 1980

If we eliminate the anomalous results of January, February, March, and December, we find that the DISC model has a significantly better %MBE than the ETMY model for Bismarck. Furthermore, the %RMSE for the DISC model indicates better performance during all months for which ground snow cover is not a problem. Furthermore, under clear atmospheric conditions, the plot of hourly errors shown on Figure 4-19 indicate that the air-mass function employed with the DISC model has effectively reduced the diurnal variations observed for the ETMY model.

5.0 CONCLUSIONS AND FUTURE RESEARCH

The DISC model employs a direct insolation simulation code that calculates the solar beam insolation incident on the surface of the earth. This model is described as a quasi-physical model, based on the following premises:

- A physical model is used to calculate clear-sky limits for the atmospheric solar radiation beam transmittance (K_{nc}).
- Deviations from clear transmittance values (ΔK_n) are calculated using an exponential function of air mass, similar in form to physical equations used in calculating energy transmission or propagation losses.
- The equations for calculating ΔK_n , K_n , and I_n are continuously variable relative to K_t and air mass; thus, they result in values that are in close agreement with real-world variations in the relationship between direct normal and global horizontal insolation.

The model does not qualify as a rigorous physical algorithm, because the coefficients for calculating ΔK_n were derived from empirical regression analyses. Nevertheless, since this model is based on physical principles, the addition of functions to account for the effects of cloud cover, precipitable water vapor, surface albedo, and atmospheric turbidity should be straightforward and effective.

5.1 Verification and Validation Results

The DISC model was verified and compared with the ETMY model using the same Atlanta data employed in developing the model. We validated and compared it with the ETMY model using data from three NOAA Solar Radiation Stations located in Brownsville, Tex.; Albuquerque, N.M.; and Bismarck, N.D. Both the verification and validation results represent significant improvements over the ETMY model. These improvements include the following:

- RMS errors have decreased for almost all station-months for the wide range of seasonal, climatological, and geographic conditions found at four sites: the maximum decrease in RMSE was 33% for Atlanta in August; the maximum increase in RMSE was 10.8% at Bismarck in December; the mean reduction in RMSE for all 48 station-months was 7.0%.
- The MBE values for the DISC and ETMY models were very similar. The mean of the absolute value of the monthly MBE was 24 W/m^2 for the DISC model and 24.5 W/m^2 for the ETMY model.
- The diurnal variations of the differences between measured and modeled values were greatly reduced for the DISC model, especially under clear-sky conditions when the direct normal irradiance is the highest.
- The improved performance of the DISC model was accomplished without changing or adjusting the model to compensate for seasonal, climatic, or geographic differences. This was possible because of the quasi-physical nature of the model, which automatically adjusts to changes in the relationship between the global horizontal and direct normal insolation components.

5.2 Future Research

During the next few years, the relationships between K_n , K_t , and air mass will be examined as a function of cloud cover, precipitable water vapor, surface albedo, and turbidity. Improvements in the DISC model will be sought for situations in which only global horizontal insolation and seasonal averages of meteorological parameters are available, and for situations in which hourly meteorological values have been collected concurrently with the global horizontal insolation data. The results to date give us every reason to believe that very significant improvements can be made in the performance of the model.

6.0 REFERENCES

- Bird, R. E., 1985, Private communications.
- Bird, R. E., and R. L. Hulstrom, 1981, A Simplified Clear Sky Model for Direct and Diffuse Insolation on Horizontal Surfaces, SERI/TR-642-761, Golden, CO: Solar Energy Research Institute.
- Bruno, R., 1978, "A Correction Procedure for Separating Direct and Diffuse Insolation on a Horizontal Surface," Solar Energy, Vol. 20, pp. 97-100.
- Bugler, J. W., 1977, "The Determination of Hourly Insolation on an Inclined Plane Using a Diffuse Irradiance Model Based on Hourly Measured Global Horizontal Insolation," Solar Energy, Vol. 19, pp. 477-491.
- Collares-Pereira, M., and A. Rabl, 1979, "The Average Distribution of Solar Radiation -- Correlations Between Diffuse and Hemispherical and Between Daily and Hourly Insolation Values," Solar Energy, Vol. 22, pp. 155-164.
- Garrison, J. D., 1985, "A Study of the Division of Global Irradiance into Direct and Diffuse Irradiance at Thirty Three U.S. Sites," Proc. INTERSOL 85, Montreal, Canada, June 23-29, 1985.
- Gordon, J. M., and M. Hochman, 1984, "On Correlations Between Beam and Global Radiation," Solar Energy, Vol. 32, pp. 329-336.
- Hall, I. J., et al., 1980, Solar Radiation Model Validation, SAND80-1755, Albuquerque, NM: Sandia National Laboratories.
- Hickey, J. R., H. L. Kyle, B. M. Alton, and E. R. Major, 1986, "ERB NIMBUS 7 Solar Measurements: 7 Years," 6th Conference on Atmospheric Radiation, American Meteorological Society, Williamsburg, VA, May 13-16, 1986.
- Iqbal, M., 1980, "Prediction of Hourly Diffuse Solar Radiation from Measured Hourly Global Radiation on a Horizontal Surface," Solar Energy, Vol. 24, pp. 491-503.
- Jeter, S. M., and C. A. Balaras, 1986, "A Regression Model for the Beam Transmittance of the Atmosphere Based on Data for Shenandoah, GA," Solar Energy, Vol. 37, No. 1, pp. 7-14.
- Jeter, S. M., and C. A. Balaras, 1987, "A Seasonal Regression Model for the Beam Transmittance of the Atmosphere," submitted to ASES Annual Meeting, 1987.
- Kasten, F., 1966, A New Table and Approximation Formula for the Relative Optical Air Mass, Technical Report 136, Hanover, N.H.: U.S. Army Material Command, CRREL.
- Liu, B. Y. H., and R. C. Jordan, 1960, "The Interrelationship and Characteristic Distribution of Direct, Diffuse and Total Solar Radiation," Solar Energy, Vol. IV, No. 3, pp. 1-19.

- Maxwell, E. L., 1987, A Plan to Upgrade the National Insolation Data Bases, SERI/PR-215-3010, Golden, CO: Solar Energy Research Institute.
- Maxwell, E. L., and R. E. Bird, 1987, An Evaluation of Direct Normal Models and Data Bases, Golden, CO: Solar Energy Research Institute, in preparation.
- Orgill, J. F., and K. G. T. Hollands, 1977, "Correlation Equation for Hourly Diffuse Radiation on a Horizontal Surface," Solar Energy, Vol. 19, pp. 357-359.
- Randall, C. M., and J. M. Biddle, 1981, Hourly Estimates of Direct Insolation: Computer Code ADIPA User's Guide, Aerospace Report No. ATR-81(7878)-1, 1 September 1981, El Segundo, CA: The Aerospace Corporation.
- Randall, C. M., and R. E. Bird, 1987, Insolation Models and Algorithms, Vol. II, Book 1, Chapter 4, DOE Solar Thermal Energy Conversion Technology Status and Assessment Project, in preparation.
- Randall, C. M., and M. E. Whitson, Jr., 1977, Hourly Insolation and Meteorological Data Bases Including Improved Direct Insolation Estimates, Aerospace Report No. ATR-78(7592)-1, 1 December 1977, El Segundo, CA: The Aerospace Corporation.
- SOLMET, 1978, User's Manual, Vol. 1, Final Report TD-9724, Asheville, NC: National Climate Center.
- Spencer, J. W., 1971, "Fourier Series Representation of the Position of the Sun," Search, Vol. 2, No. 5, pp. 172.
- Vignola, F., and D. K. McDaniels, 1984, "Correlations Between Diffuse and Global Insolation for the Pacific Northwest," Solar Energy, Vol. 32, pp. 161-168.
- Vignola, F., and D. K. McDaniels, 1986, "Beam-Global Correlations in the Pacific Northwest," Solar Energy, Vol. 36, No. 5, pp. 409-418.
- WMO, 1981, Meteorological Aspects of the Utilization of Solar Radiation as an Energy Source, Tech. Note No. 172, WMO-No. 557, World Meteorological Organization, Geneva, Switzerland.

Document Control Page	1. SERI Report No. SERI/TR-215-3087	2. NTIS Accession No.	3. Recipient's Accession No.
4. Title and Subtitle A Quasi Physical Model for Converting Global Horizontal to Direct Normal Insolation	5. Publication Date August 1987		6.
	7. Author(s) Eugene L. Maxwell		8. Performing Organization Rept. No.
9. Performing Organization Name and Address Solar Energy Research Institute A Division of Midwest Research Institute]6]7 Cole Blvd. Golden, Colorado 8040]-3393	10. Project/Task/Work Unit No. 6003.100		11. Contract (C) or Grant (G) No. (C) (G)
	12. Sponsoring Organization Name and Address		13. Type of Report & Period Covered Technical Report 14.
15. Supplementary Notes			
16. Abstract (Limit: 200 words) Numerous research studies have shown that the use of a single regression function does not adequately characterize the relationship between direct beam transmittance (Kn) and the effective global horizontal transmittance (Kt). Therefore, the Direct Insolation Simulation Code (DISC) employs an exponential relationship between ΔKn and air mass which is parametric in Kt. This algorithm seems to provide a satisfactory Kn-Kt relationship for a wide range of stations and seasons. Validation of the DISC Model was accomplished with data from three widely separated stations (Albuquerque, Bismarck, and Brownsville) which were not used for model development. Comparisons with the ETMY model (used to generate direct normal data for 222 of the 248 stations in the national data base) showed substantial improvements in the accuracy of hourly values, significant reductions in monthly RMS errors, and equivalent monthly mean bias errors. Furthermore, modification of the DISC model to incorporate cloud-cover, water vapor, and albedo terms appears to be straightforward.			
17. Document Analysis a. Descriptors solar radiation; insolation; solar irradiance; resource assessment b. Identifiers/Open-Ended Terms c. UC Categories 62, 63			
18. Availability Statement National Technical Information Service U.S. Department of Commerce 5285 Port Royal Road Springfield, Virginia 22161		19. No. of Pages 67	
		20. Price A04	